SPECIAL
GDIS Drought Worldwide
COLLECTION

Northern Eurasian Heat Waves and Droughts

SIEGFRIED D. SCHUBERT, HAILAN WANG,* RANDAL D. KOSTER, AND MAX J. SUAREZ

Global Modeling and Assimilation Office, NASA GSFC, Greenbelt, Maryland

PAVEL YA. GROISMAN

National Climatic Data Center, Asheville, North Carolina

(Manuscript received 25 June 2013, in final form 25 December 2013)

ABSTRACT

This article reviews the understanding of the characteristics and causes of northern Eurasian summertime heat waves and droughts. Additional insights into the nature of temperature and precipitation variability in Eurasia on monthly to decadal time scales and into the causes and predictability of the most extreme events are gained from the latest generation of reanalyses and from supplemental simulations with the NASA Goddard Earth Observing System model, version 5 (GEOS-5). Key new results are 1) the identification of the important role of summertime stationary Rossby waves in the development of the leading patterns of monthly Eurasian surface temperature and precipitation variability (including the development of extreme events such as the 2010 Russian heat wave); 2) an assessment of the mean temperature and precipitation changes that have occurred over northern Eurasia in the last three decades and their connections to decadal variability and global trends in SST; and 3) the quantification (via a case study) of the predictability of the most extreme simulated heat wave/drought events, with some focus on the role of soil moisture in the development and maintenance of such events. A literature survey indicates a general consensus that the future holds an enhanced probability of heat waves across northern Eurasia, while there is less agreement regarding future drought, reflecting a greater uncertainty in soil moisture and precipitation projections. Substantial uncertainties remain in the understanding of heat waves and drought, including the nature of the interactions between the short-term atmospheric variability associated with such extremes and the longer-term variability and trends associated with soil moisture feedbacks, SST anomalies, and an overall warming world.

1. Introduction

"While in western Europe there is continual rain and they complain about the cold summer, here in Russia there is a terrible drought. In southern Russia all the cereal and fruit crops have died, and around St Petersburg the forest fires are such that in the city itself, especially in the evening, there is a thick haze of smoke and a smell of burning. Yesterday, the burning woods and peat bogs threatened the ammunition stores of the artillery range and even the Okhtensk gunpowder factory" (http://therese-phil.livejournal.com/171196.html). This remarkable 15 July 1875 entry in General Dmitry Milyutin's diary reflects not only the fact that Russia suffered from terrible drought and heat in the past, but also a realization long ago that such droughts were at times juxtaposed with cool and wet conditions over Europe. Today, we know this juxtaposition is no coincidence but in fact reflects the unique large-scale atmospheric controls on drought and heat waves affecting much of northern Eurasia. Droughts in Eurasia indeed have a character all their own.

Historical records show that over time the peoples of the Eurasian continent have suffered through

* Additional affiliation: Science Systems and Applications, Inc., Lanham, Maryland.

Corresponding author address: Siegfried Schubert, NASA/GSFC, Global Modeling and Assimilation Office, NASA/GSFC Code 610.1, Greenbelt, MD 20771.
E-mail: siegfried.d.schubert@nasa.gov

DOI: 10.1175/JCLI-D-13-00360.1

© 2014 American Meteorological Society

numerous heat waves and droughts, events that have impacted the course of battles,[1] desiccated important crop lands (thereby inducing famine), produced numerous forest and peat fires, and contributed to thousands of deaths. Gumilev (1960) and Pines (2012) review the pulses of dry and relatively humid periods that have occurred during the past two millennia over the entire Great Steppe of northern Eurasia (from Pannonia in the west to Manchuria in the east), causing prosperity and decay of ancient states and the migration of nomadic tribes. A compendium of extreme events during the past 1100 years over ancient European Russia (ER), Belarus, and Ukraine (so-called Kiev Rus') is provided by Borisenkov and Pasetsky (1988), Bogolepov (1922), and Vazhov (1961). Appendix B contains a list of the major droughts and heat waves that have occurred since the late nineteenth century.

Droughts continue to have major impacts on northern Eurasian agriculture. As noted in Golubev and Dronin (2004), "Another notable feature of Russian agriculture are the rather large fluctuations in year-to-year yield, which are considerably higher than in any other major grain producing country in the world... These high fluctuations in total cereal production were undoubtedly the result of irregular precipitation." In fact, many of the important early studies on Russian drought and temperature extremes were performed to address their impacts on agriculture in the important growing regions of Povolzhie, the North Caucasus, and the Central Chernozem Region, regions that produce about ⅔ of the Russian food grains (Kleschenko et al. 2005). Kahan (1989) lists some major Russian droughts [based on the work of Rudenko (1958); see also our appendix B] and their agricultural impacts; he notes that the increased impact of natural calamities was in part associated with the expansion of Russian agriculture (mainly grain acreage) toward the south and southeast into the steppes and semiarid regions characterized by drier climatic conditions. However, these regions are also characterized by fertile soils (chernozem, sometimes called "black earth") and have longer growing seasons.[2] This, together with a general increase of grain productivity, appears to have made the severe drought-induced famines of previous years much less likely. For example, the 2010 heat wave and drought over ER (which was so severe that we had to go back to AD 1092 to find an analog)[3] did not cause a famine but did cause a stoppage of grain export from Russia. Multiple-year droughts have occurred over the past century, especially in the heartland of the Eurasian steppes (Kahan 1989). Such droughts include the 5-yr event (1929–33) in the Akmolinsk (presently Astana, the capital of Kazakhstan) area. Historically, famines, when they occur, tend to be associated with multiple years of drought (Borisenkov and Pasetsky 1988).

An interesting and telling aspect of the literature addressing droughts in northern Eurasia is the lack therein of a clear distinction between drought and heat waves. To some extent, this is because summer dryness in this region has two different manifestations: agricultural drought (i.e., soil moisture deficits) and "fire weather" (in the forested areas of northern Eurasia, a prolonged period of hot weather with little or no rainfall) as described in, for example, Nesterov (1949) and Groisman et al. (2007). Agricultural droughts in northern Eurasia also may last for several weeks or even months, particularly

[1] The town of Szigetvár, Hungary, was under siege by the Turks on 7 August 1566. The main protection of the town was a lake and marshland that normally surrounded it. "Chance however now favored the Turks. A drought had prevailed during the two preceding months, and the terrain surrounding the old town had become so dry, as considerably to facilitate the approach of the enemy." Vámbéry (1886, p. 314).

[2] For example, when at the end of the rule of Tsar Boris Godunov the Moscow Tsarstvo was struck by a 3-yr-long famine (1601–03), cold summers were to blame, most probably related to a catastrophic volcanic eruption of Huaynaputina (Peru) in 1600. At that time the present major grain areas of ER were not plowed and the present region of "sustainable agriculture" in the forested areas of central ER around 55°N simply did not receive summer temperatures sufficient for grain harvests. Ultimately, this famine caused an 8-yr-long period of social turmoil, civil war, and invasion by Swedish and Polish marauders, and it ultimately caused a change in the ruling dynasty.

[3] National Yearbooks (Letopisi) prepared by Russian monks since the early tenth century report most important political and environmental events over Kiev Rus' (the area of present northern Ukraine, eastern Belarus, and the central part of European Russia). In the twentieth century, Letopisi were summed and reanalyzed (Borisenkov and Pasetsky 1988; Barash 1989). Generally, summers over Kiev Rus' in the eleventh century were mostly warm and dry. However, on this background, the 1092 summer was extremely dry. The Moscow Letopisi summary for 1092 says: "Huge circle was in the sky in this summer, a drought was so strong that soil was burned and many forest and swamps were set in fire themselves." Letopisi witness: clear skies throughout the entire summer; prolonged period without rainfall; extremely hot weather; fields and pasture "fired out," and widespread naturally caused forest and peat bog fires (let us recall that at that time wetlands were undisturbed, which is opposite to the present state of affairs). In Kiev, in the following autumn and winter more than 7000 (of total 50 000) died from starvation. Losses beyond the capital city were (in percent) even higher. This unfortunate development was followed by widespread epidemics.

under conditions of a short growing season when a complete harvest loss can be caused by a short heat wave that strikes at a critical period of wheat development. Another aspect of droughts in the steppe and semidesert zones of northern Eurasia are "sukhovey"—extended periods of dry hot winds characterized by intense transpiration and rapid wilting of vegetation (Lydolph 1964). Sukhovey typically emanate from the periphery of anticyclones, bringing in warm and dry air originating in the deserts of Africa, Asia Minor, and southern Kazakhstan (http://en.wikipedia.org/wiki/Sukhovey). Historically, sukhovey have been a major impediment to large-scale sedentary agriculture in Central Asia (Sinor 1994). An important point here is that the traditional notions of meteorological (precipitation deficits) and agricultural droughts (soil moisture deficits) are perhaps not as relevant or as clearly separated in northern Eurasia as in other regions of the world.

The strong link between heat waves and drought in northern Eurasia suggests that we should treat them as different facets of the same phenomenon. In fact, many metrics of drought in northern Eurasia involve an explicit temperature criterion; a drought is said to occur, for example, only after a certain minimum number of days with temperatures above a certain threshold (e.g., Selianinov 1928). The strong connection between drought and excessive heat reflects in part the central role of anticyclones in the development of northern Eurasian droughts; the anticyclone inhibits precipitation by blocking or diverting the westerlies and storm systems, and it increases temperature through descending motions (which further inhibit precipitation) and increased insolation associated with clear skies (e.g., Buchinsky 1976). Another relevant mechanism involves soil moisture feedback on temperature; reduced precipitation leads to reduced evaporative cooling of the land surface. While multiyear droughts do occur in Eurasia, particularly toward the south of our study area, most droughts have shorter time scales; most severe events[4] occurring across northern Eurasia in fact rarely exceed 50 days in duration (Cherenkova 2007). The north/south differences and east/west differences in drought occurrence reflect the spatially varying influences of the oceans and various air masses (tropical, subtropical, and polar) across the continent and the arrangement of Eurasia's major mountain chains.

[4] However, as mentioned above, it is enough in this part of the world to have several days of adverse weather during particular periods of cereal growth to cause crop loss. Such short-term events (waves) are much more frequent than long periods of decremented weather.

The recent extreme heat waves and droughts of 2003 (Europe) and 2010 (Russia) have highlighted the urgency of understanding better their causes and whether or not they are a manifestation of a warming world (e.g., Dole et al. 2011; Trenberth and Fasullo 2012; Otto et al. 2012). While there is agreement on many aspects of such extreme events, including the role of anticyclones, there are still substantial unknowns about their causes and predictability. In particular, we do not yet understand which large-scale processes (including climate change, SST, monsoons, links to higher latitudes) may have played a role in making them so exceptional.

In this paper, we delve into some of the outstanding questions regarding the nature and causes of Eurasian heat waves and droughts, their predictability, and what we can expect in a future warmer world. We focus on northern Eurasia, in particular the region outlined in the Northern Eurasia Earth Science Partnership Initiative (NEESPI; Groisman et al. 2009)—longitudinally, this region extends from 15°E to the Pacific coast, and latitudinally it extends from 40°N to the Arctic Ocean coastal zone. The region includes the territory of the former Soviet Union, Fennoscandia, eastern Europe, Mongolia, and northern China, although our presentation of the results often extends beyond it in order to provide a more global perspective of relevant teleconnections and physical mechanisms.

This paper is part of a Global Drought Information System (GDIS) special collection that addresses the causes of drought worldwide. We note that there are separate papers in this collection focusing on drought in large regions bordering and in part overlapping northern Eurasia, including papers on Europe, the Middle East, southwest Asia, and eastern Asia (e.g., Barlow et al. 2013, manuscript submitted to *J. Climate*; Zhang and Zhou 2014, manuscript submitted to *J. Climate*). The interested reader is referred to those papers for more information on those regions. In keeping with the guidelines of the submissions to the GDIS special collection, we will touch on the following topics: i) drought/heat wave occurrence, metrics, and impacts; ii) key regional circulation features and physical processes; iii) trends; iv) predictability and projections; and v) gaps in our understanding.

We begin in section 2 by discussing the morphology and metrics of droughts and heat waves. Section 3 examines the physical mechanisms responsible for their occurrence. Section 4 contains a review and analysis of interannual variability and trends, and section 5 discusses projections and predictability. A summary is provided in section 6. In addition, two appendices are provided: Appendix A describes the datasets and model simulations used in this study, and appendix B provides a compilation (based on various sources including research papers and the popular literature) of some of the major droughts and

heat waves that have occurred in northern Eurasia since 1875.

2. The morphology and metrics of northern Eurasian heat waves and droughts

a. Characterizing drought and heat waves

The previous discussion highlighted the adverse impacts of prolonged drought conditions, as well as shorter-period (from weeks to months) heat waves and related droughts, on the main agriculture regions of northern Eurasia, with the latter events also playing an important role in the occurrence of "fire weather" in the forested areas of northern Eurasia. The discussion also emphasized the importance of the interplay between temperature and precipitation variability in the development of droughts. Droughts are ultimately driven by precipitation deficits, and their impacts (e.g., on agriculture) depend on the extent to which they lead to deficits in soil moisture and other water resources important to society. Temperature increases associated with the precipitation reductions, which can act to exacerbate the drought conditions, can result from reductions in cloudiness; reduced cloud cover over northern Eurasia in summer can warm the surface, since daytime warming is 2–3 times stronger than the nighttime cooling, and the period of daylight is longer than the period of nighttime (Groisman et al. 1999; Tang et al. 2012; Tang and Leng 2012, 2013). The temperature increases can also result from reductions in soil moisture, which lead to reduced evaporation and thus reduced evaporative cooling of the surface. Finally, various dynamical processes linked to (for example) the development of persistent anticyclones (the subject of the next section) can act to further reduce cloudiness and precipitation and at times can lead to intense heat waves.

Here we look at various measures that highlight and quantify the above aspects of droughts and heat waves over northern Eurasia. A number of different indices are available for consideration. Most are based on joint consideration of precipitation and temperature, with a focus on agricultural applications (e.g., Meshcherskaya and Blazhevich 1997; Kleschenko et al. 2005); examples include the hydrothermal coefficient (HTC; Selianinov 1928) and the dryness index of Ped (1975). Meshcherskaya and Blazhevich (1997) developed a combined drought and excessive moisture index (DM) that takes into account the areal extent of the precipitation and temperature anomalies. Appendix B provides more details on these and several other of the more popular metrics.

The overall character of northern Eurasian precipitation and temperature variability and its relationship to drought and heat waves is now examined. Figure 1 (left panels) shows the variance of June–August (JJA) mean precipitation for the last three decades (1979–2012) as determined by two different reanalyses and from an analysis of station observations. While there are some differences, there is general agreement that the largest precipitation variance over northern Eurasia occurs over European Russia extending eastward along about 55°N—a region for which the maximum rainfall in summer is associated with cyclones from the Atlantic reaching the Yenissey River Valley in central Siberia. Other regions with relatively large precipitation variance are found in the west Caucasus and in the mountainous regions of southeastern Russia/northeast China. Minimum variances are seen in the desert regions east of the Caspian Sea extending to northwestern China and Mongolia.

While a precipitation deficit is the basic ingredient of drought, the link between the magnitude of such deficits and the presence of drought, at least as defined by established drought indices, is not readily apparent. To make this link quantitative we take as an example the connection of the precipitation deficits with the Ped (1975) dryness index, S_i (the difference between the normalized anomalies of JJA-mean surface temperature and precipitation; see appendix B for definitions). The variance of S_i is

$$V = 2(1 - \rho), \tag{1}$$

where ρ is the correlation between the surface temperature and precipitation. The variance in drought as measured by the Ped (1975) dryness index thus highlights the fact that drought depends on the interplay between precipitation (P) and temperature (T). Figure 1 compares the variance field for the drought index (right panels) to that for precipitation (left panels). Note that a comparison of the magnitudes is irrelevant, since the fields have different units; here, we consider only the comparison of spatial patterns. For the dryness index, the largest values (regions with the largest negative correlations between P and T) occur farther south, extending across the main agricultural regions of northern Eurasia, as well as over much of Mongolia and northeast China. Consistent across the three estimates are the relatively large values to the north and east of the Caspian Sea (including northern Kazakhstan), over the Caucasus, and over much of Europe, including the Balkans. In essence, the comparison in Fig. 1 shows that standard drought indices do not simply describe the absolute magnitudes of precipitation deficits but, as we shall see in Fig. 2, also reflect the important link with temperature.

We note that the coefficient of variation (C_v) relates precipitation fluctuations to mean or "normal" climate

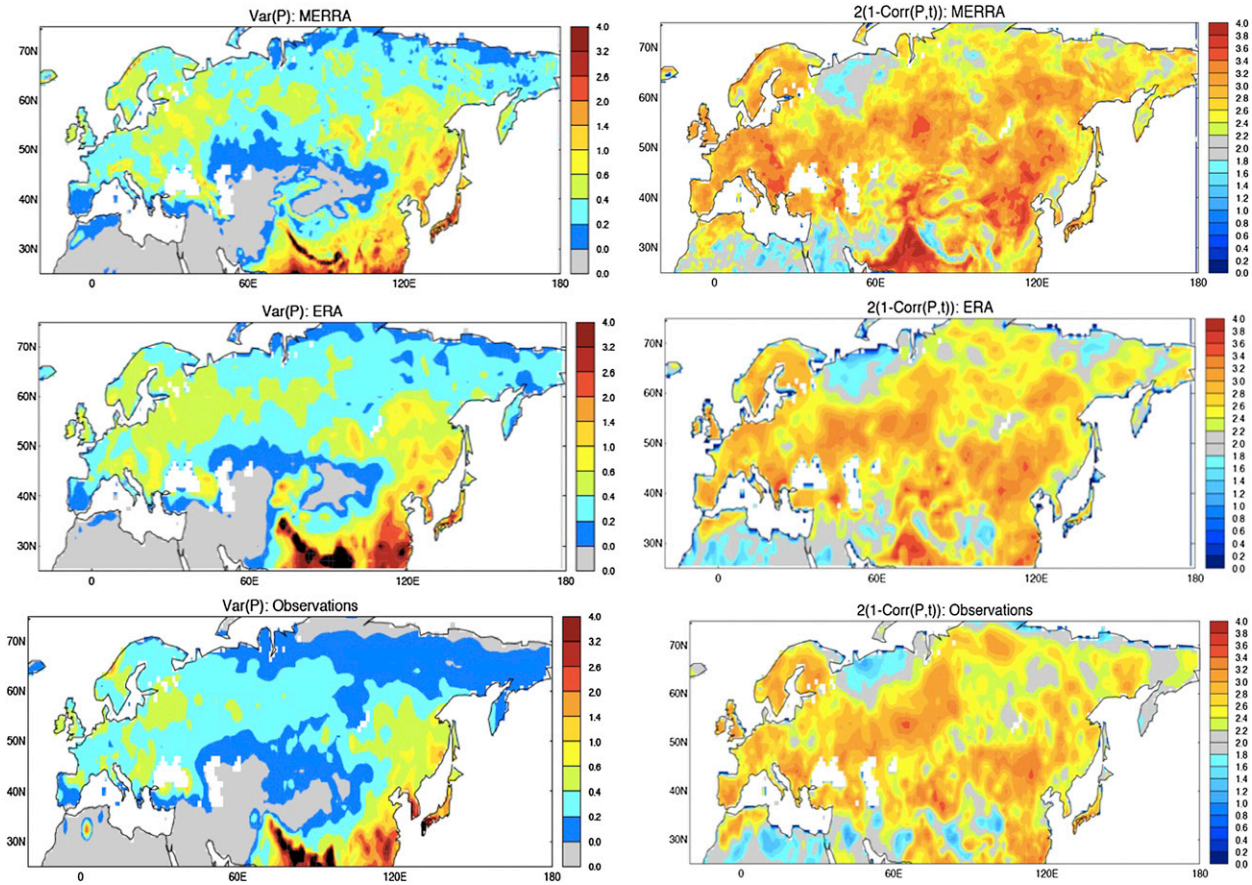

FIG. 1. (left) The mean JJA precipitation variance from MERRA, ERA-Interim, and NOAA-PRECL observations, computed for the period 1979–2012. Units are (mm day^{-1})^2. A linear trend was removed for each calendar month before computing the variances. (right) As at (left), but for the variance of the Ped (1975) drought index (see text).

values—a metric that is in principle[5] perhaps a better measure of precipitation irregularity as it relates to potential impacts on agriculture. Shver (1976) showed, for example, that while C_v values of monthly rainfall totals over Eurasian agricultural areas north of 55°N from May to July are close to 0.5, farther south C_v gradually increases and in the North Caucasus, southern Ukraine, and northern Kazakhstan reaches values of 0.7 in July and 0.8 in August, indicating that the latter regions experience larger swings in precipitation relative to the mean.

We next turn to the temperature variance. The left panels of Fig. 2 show that the variance of the JJA mean is characterized by generally increasing values with latitude, with the largest variance occurring north of the Caspian Sea and over the Ural Mountains. While this looks nothing like the distribution of the precipitation variance (Fig. 1, left panels), we have already seen that there are regions where the precipitation and temperature are correlated (Fig. 1, right panels). We can quantify the extent to which the temperature variability is "explained" by precipitation variability via simple linear regression. The results (right panels of Fig. 2) indicate that precipitation variability explains a substantial fraction of the temperature variance over much of southern European Russia and western Siberia (e.g., through evaporative cooling). The similarity to the variance of the Ped index (cf. Fig. 1, right panels) is not surprising since both measures depend on the correlation between the temperature and precipitation. Furthermore these regions occur in the transition between so-called water-limited (to the south) and energy-limited (to the north) climate regimes (Koster et al. 2006a, their Fig. 4a), where land feedbacks are particularly important (Koster et al. 2004). We will look more directly at the impact of soil moisture feedbacks on temperature variability in the context of model simulations in section 3.

[5] In practice this metric is sensitive to bias in the estimates of the mean state.

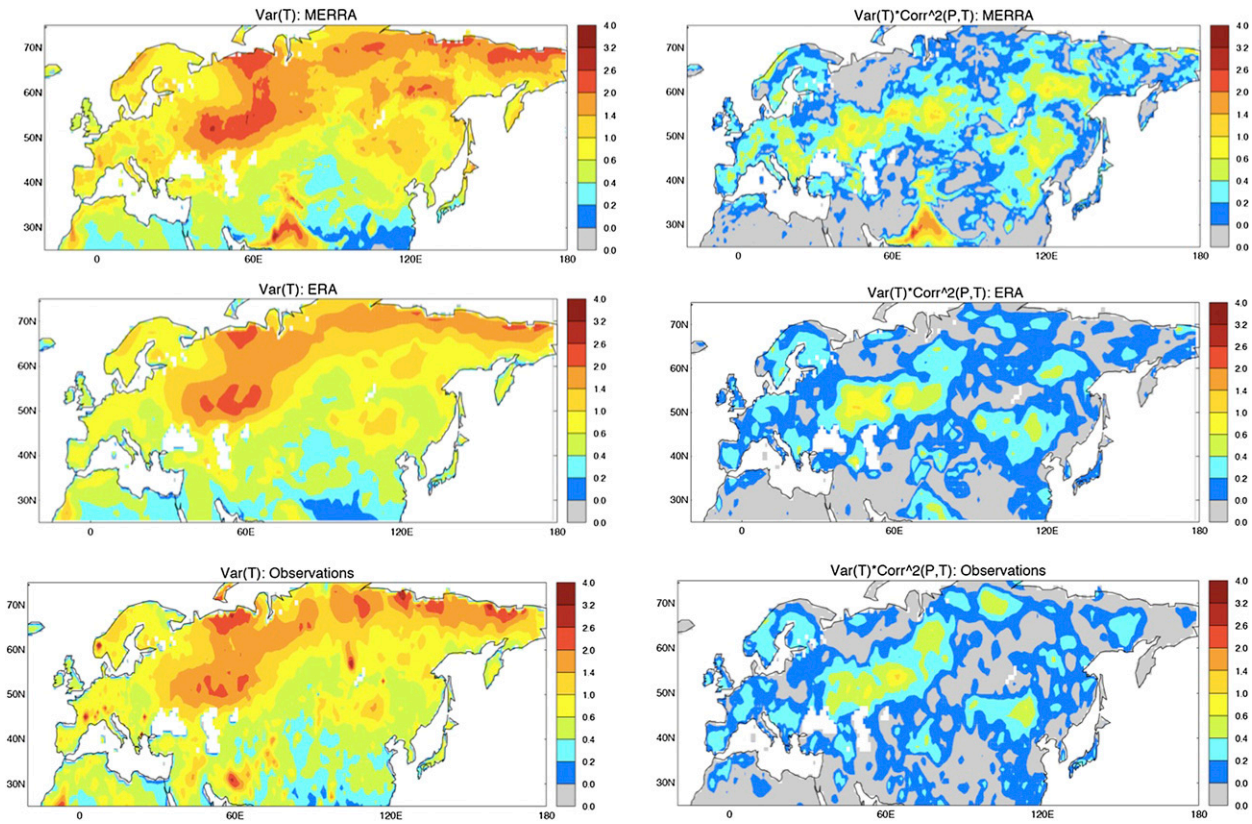

FIG. 2. (left) The mean JJA 2-m temperature variance from MERRA, ERA-Interim, and GHCN CAMS observations, computed for the period 1979–2012. Units are $(°C)^2$. A linear trend was removed for each calendar month before computing the variances. (right) As at (left), but for the percent of the 2-m temperature variance explained by precipitation (see text).

Of course, as mentioned above, cloud cover can also affect temperature variability. In fact, in an assessment of the role of cloud cover and rainfall on the daytime temperature (T_{max}), Tang et al. (2012) showed that for the western half of northern Eurasia (where the major agricultural regions reside), summer cloud cover is negatively correlated with T_{max} and that these correlations are much stronger than those with precipitation. Tang and Leng (2012) show that the variance of Eurasian summer T_{max} is better explained by changes in cloud cover than by changes in precipitation at high latitudes and in the midlatitude semihumid area, while in northern Eurasia the dependence on precipitation is strong only in the Central Asia arid area.

The above findings suggest that heat waves in northern Eurasia are influenced by both soil moisture (and precipitation) and circulation (and cloud cover) anomalies, although it is still unclear which plays the more important role. The interactions involved are indeed complex; precipitation deficits can be caused by decreases in cloudiness, and a dry land surface can suppress evapotranspiration and thus inhibit local cloud formation. All said, it seems reasonable to pay significant attention to the atmospheric factors affecting dry weather (at least for heat waves), such as the cyclones and anticyclones that control cloud cover over most of the northern extratropics.

b. *Persistent anticyclones*

The key role of anticyclones in generating Eurasian drought and heat waves has important implications for their spatial structures and time scales. In Eurasia, severe drought conditions in one region (say, European Russia) are at times accompanied by wet and cool conditions to the west over Europe and/or to the east over parts of Siberia. This is suggestive of an east–west wave structure underlying the surface temperature and precipitation anomalies and thus of strong atmospheric controls. Such structures are evident in the analysis of Eurasian heat waves provided by Gershunov and Douville (2008). They note that "In both model and observations, there is a strong interannual propensity for far eastern Europe to be cold during heat wave summers in west-central Europe. Both recent extreme European heat wave summers of 1994 and 2003 were cold in far-eastern Europe and warm over north-central Siberia, thus exhibiting Eurasian summer temperature wave train

conditions typical of large European heat waves.'' Stankūnavičius et al. (2012) carried out an empirical orthogonal function (EOF) analysis of surface air temperature (SAT) and sea level pressure (SLP) for every (2 month) season over Eurasia based on National Centers for Environmental Prediction (NCEP)–National Center for Atmospheric Research (NCAR) reanalyses for the second half of the twentieth century. They found clear evidence of wave structures in the leading modes of SAT variability during early and late summer. Sato and Takahashi (2006) identified a southern Eurasian wave train extending far enough eastward to affect Japan.

Using NCEP–NCAR reanalysis data, Stefanon et al. (2012), with a clustering approach, identified six major types of European heat waves for the period 1950–2009. The types found include a Russian cluster, a Scandinavian cluster, a western European cluster, and an eastern European cluster, with the temperature anomalies in phase with the anticyclonic (positive 500-mb geopotential height) anomalies. They found that drought appears to be a prerequisite to heat wave occurrence in western and eastern European heat waves (rainfall deficits in southern Europe), but not for the more northerly Russian or Scandinavian heat waves (see section 3 below).

c. *The leading modes of surface temperature and precipitation covariability*

The above studies on drought and heat wave characteristics suggest that we can effectively quantify hydrodynamical variability over Eurasia in terms of the *combined* monthly temperature and precipitation variability. To do this efficiently, we employ a rotated[6] empirical orthogonal function (REOF) analysis. The basic quantities used in the calculation of the REOFs (the normalized monthly temperature and precipitation fields) are the same as those used in the calculation of the Ped (1975) drought index (section 2a). We focus here on monthly rather than seasonal means to better capture the variability associated with persistent large-scale atmospheric waves.

The first REOF (top panels of Fig. 3) shows a clear wave structure in both the temperature and precipitation, with anomalies of alternating sign spanning Eurasia (both across the north over Siberia and to the south into China). The greatest temperature loading (shown here as positive) is centered on European Russia (the European Plain) west of the Ural Mountains. The associated precipitation loadings have negative values on the southeastern quadrant of the main warm anomaly (just north of the Caspian Sea), suggestive of a dynamical link between the temperature and precipitation anomalies. Positive values for precipitation occur over central Europe, Scandinavia, northern Siberia, and mountains of Central Asia. The corresponding time series of the leading REOF [referred to as the rotated principal component (RPC)] in Fig. 4 show that this pattern is associated with a trend toward more positive values over the last 30 years; it thus appears to have played an important role in the Russian heat wave of 2010 (relatively large positive values for June, July, and August).

The second REOF again shows a wave structure, with the largest loading in the temperature field just east of the Urals, indicating an east–west phase shift with respect to the first REOF. Positive values also occur over southern Europe, while negative values occur over Scandinavia, northeastern Europe, and much of eastern Asia. The associated precipitation loadings show negative precipitation anomalies just to the east of the Ural Mountains (again on the southeastern quadrant of the main positive temperature anomaly) and over much of Europe, while positive anomalies stretch from Scandinavia southeastward across Kazakhstan, Mongolia, and China. The associated RPCs show that this pattern was very pronounced in August of 2003, during the height of the 2003 European heat wave. We note that the first REOF was also very pronounced (negative) in 2003 although this occurred in June of that year at the start of the heat wave. The associated RPC shows no clear trend in the last three decades (Fig. 4).

REOFs 3–5 are also characterized by wave structures, with the maximum positive temperature anomalies centered just east of the Caspian Sea, just north of Mongolia, and over northern Europe, respectively. REOF 3 differs somewhat from the others in that it is indicative of a more southerly wave path. In all three cases, the main negative precipitation anomalies are either in phase or slightly to the east/southeast of the main positive temperature anomalies. The associated RPCs (particularly RPCs 3 and 4) indicate a change toward more positive values after about 1995. We will come back to the trends in section 4. In the following section, we focus on the mechanisms responsible for such wave structures.

3. Physical mechanisms

a. *A review*

As mentioned in the previous section, it has long been recognized that persistent anticyclones play a fundamental role in the generation of drought and heat waves over

[6] Rotation (Richman 1986) acts to spatially localize anomalies, and has been found by the authors to produce more physically realistic patterns of variability compared with unrotated EOFs. We note that the REOF methodology has no inherent tendency to produce wave structures; in fact, the localization would tend to deemphasize connections at large distances.

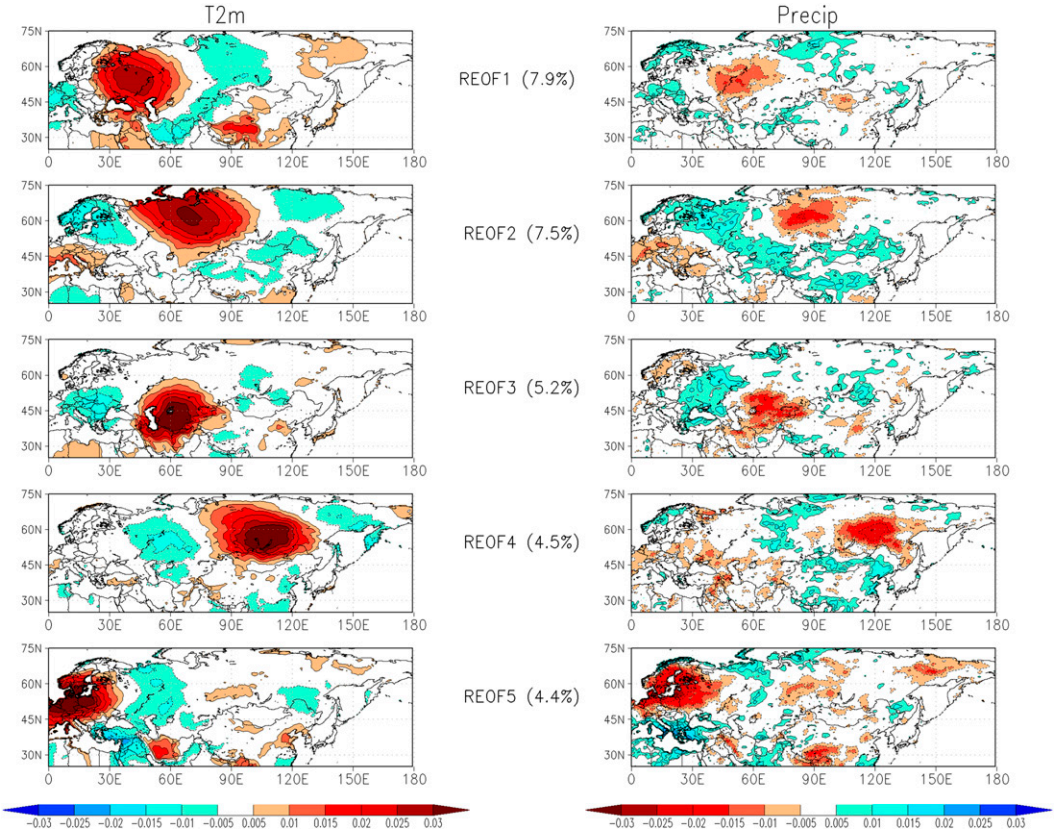

FIG. 3. The five leading rotated empirical orthogonal functions (REOFs) of the combined monthly fields of 2-m temperature and precipitation for JJA of 1979–2012. The fields are normalized by their respective variances (standard deviation) and a linear trend was removed for each calendar month before computing the REOFs. The results are based on MERRA. Units are arbitrary.

northern Eurasia. Buchinsky (1976) summarizes some of the key aspects of droughts in the central part of European Russia and the Volga region, noting that over 70% of them are associated with persistent anticyclones that act to disrupt the predominantly zonal flow and eastward progression of weather systems. He notes that these are primarily Arctic anticyclones that advance from the Barents or even the Kara Sea and become stationary over the plains. Similarly, the work of Selianinov (1928) and others, as summarized in Kleschenko et al. (2005), showed that drought in the arid regions of Russia and other Commonwealth of Independent States (CIS) regions results from the penetration of anticyclonic air masses from the Artic. They note that these anticyclones can act in concert with anticyclones at the southern (40°–50°N) and high (~75°N) latitudes. The former become more important farther to the west where, for example, Ukraine is impacted by the Azores high. They note that most often the Arctic and Azores intrusions are combined in the Lower Volga and the southern Yuzhny Ural regions, leading to pronounced drought conditions.

Similarly, eastern Europe (e.g., Poland) periodically experiences drought related to a persistent stationary anticyclone (an east European high) that joins with the Azores anticyclone via central Europe (Farat et al. 1998). As noted by Golubev and Dronin (2004) ''An especially strong drought takes place when an anticyclone is fed by an air mass from an Azores anticyclone moving in from the West. Moving across Europe, the air mass loses its humidity and reaches European Russia completely dry (Protserov 1950). The droughts resulting from these large scale atmospheric processes usually cover vast territories of Russia, including the Northern Caucasus, the Middle and Lower Volga basin, the Urals, and periodically spread over the central chernozem region and even the northern regions of European Russia. For example, the drought of 1946 covered 50 percent of total agricultural land of the USSR. As a result, the scale and consequences of droughts can be catastrophic for the country.''

The physical mechanisms that determine the persistence and scale of the northern Eurasian anticyclones are still not well understood, although atmospheric blocking

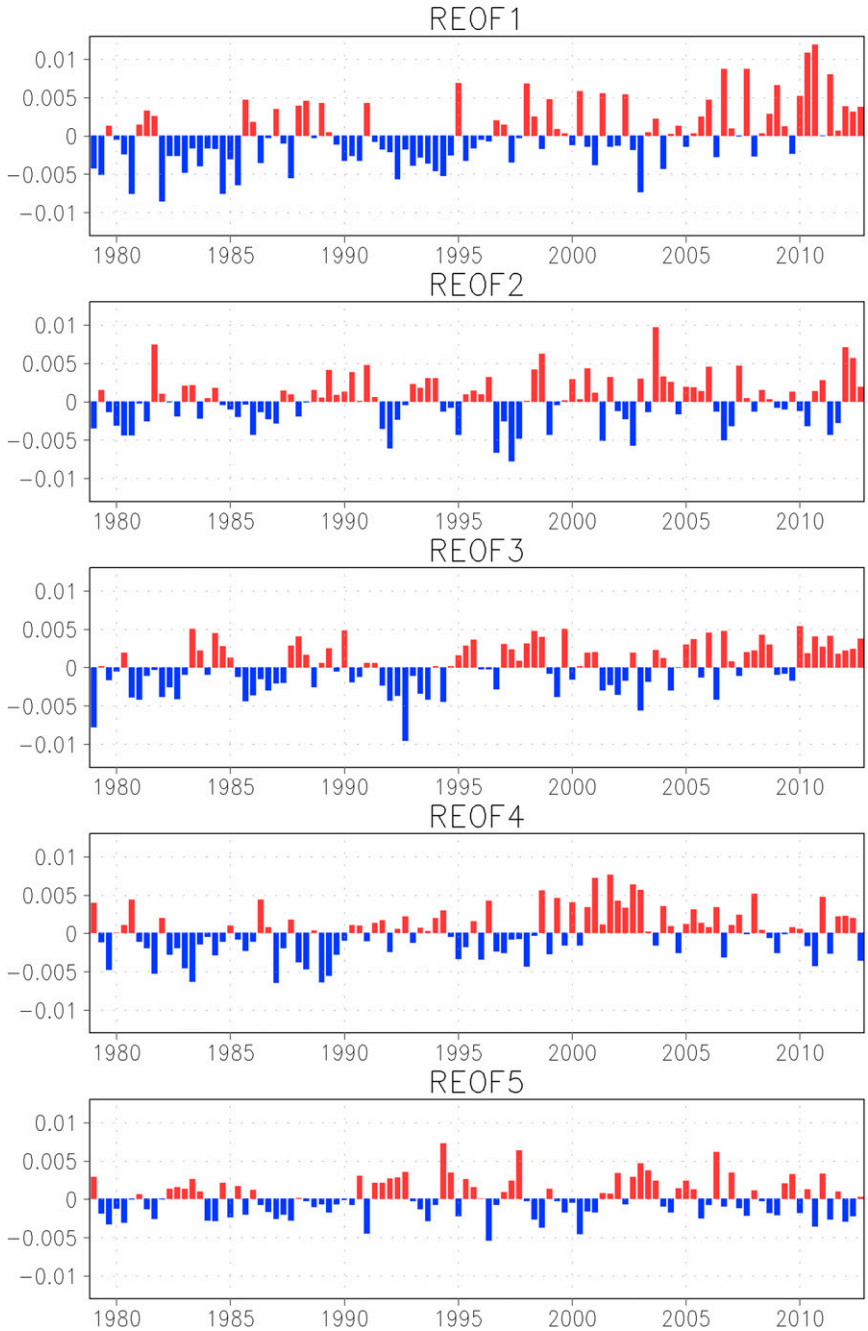

FIG. 4. The projection of the monthly JJA normalized 2-m temperature and precipitation fields onto the leading REOFs shown in Fig. 3. The fields are not detrended. The values are referred to in the text as the rotated principal components (RPCs). Units are arbitrary.

has long been considered important. Studies of blocking that focus on the Atlantic and impacts on Eurasia go back to Obukhov et al. (1984) and a number of earlier studies reviewed therein. That study in particular reviewed various potential mechanisms of blocking, including those linked to orography and the instability of the polar jet, and it emphasized atmospheric blocking as a precondition for drought in summer, with both the downward movement of air within the associated anticyclone (acting to heat and dry the air) and the blocking of the westerlies (inhibiting the inflow of moisture from the west) contributing to the drought conditions. More recently, Nakamura et al. (1997) contrasted Pacific and Atlantic blocking events and found that incoming wave

activity associated with a quasi-stationary Rossby wave train is of primary importance in the development of blocking over Europe, while the forcing from synoptic-scale transients is key for the development over the North Pacific.

In addition to blocking, a number of other large-scale modes of variability can affect northern Eurasia on weekly to monthly time scales. The important role of the northern annular mode (NAM) for Eurasian climate has been documented in numerous studies (e.g., Thompson and Wallace 2001). While many studies have focused on the winter season, others have documented the impact of the NAM on variations in land surface phenology such as the start of the growing season and the timing of the peak normalized difference vegetation index (NDVI) over northeastern Russia (e.g., de Beurs and Henebry 2008). Rocheva (2012) linked the persistent 500-mb height anomalies over European Russia and western Siberia to the eastern Atlantic/western Russia (EA/WR) and Scandinavian (SCA) patterns of variability, respectively, from May through July—patterns that are still not well understood.

Bothe et al. (2010) linked drought over Tibet to a Eurasian wave train that spans Eurasia from Scandinavia to the South China Sea. They associated the development of the wave to strong anticyclonic activity over northern Europe/Scandinavia, which in turn is supported by anomalous transient eddy activity associated with the North Atlantic storm track. Ding and Wang (2005) identified a wavenumber-5 summertime circumglobal teleconnection pattern confined to the summer jet waveguide with significant impacts on interannual (and intraseasonal; Ding and Wang 2007) temperature and precipitation variations over much of Eurasia and North America, apparently maintained by heat sources associated with the Indian monsoon. Schubert et al. (2011) examined the role of stationary Rossby waves on intraseasonal summertime variability in the Northern Hemisphere extratropics and showed that many of the extreme events, including the 2003 European and 2010 Russian heat waves, are associated with a particular recurring Eurasian stationary wave pattern that affects much of the northern Eurasian continent. This, along with other summertime wave structures, was found to be primarily forced by submonthly vorticity transients, although it was also found that the waves do at times contribute substantially to the seasonal mean anomalies, suggesting some impact from other longer-term (e.g., SST) forcing.

Uncertainties about the causes of persistent northern Eurasian anticyclones result from limitations in our understanding of the basic dynamical mechanisms involved and from uncertainties about the impact of global warming, especially in regard to the occurrence of some of the most extreme events (e.g., Dole et al. 2011; Schneidereit et al. 2012; Lau and Kim 2012; Galarneau et al. 2012; Trenberth and Fasullo 2012; Lupo et al. 2012). On the one hand, for example, Dole et al. (2011) emphasized the important role of internal midlatitude atmospheric dynamics in producing an intense and long-lived blocking event and associated anticyclone (producing the warmest July since at least 1880 in western Russia), and they concluded that neither human influences nor slowly varying ocean boundary conditions contributed substantially to the magnitude of the event. They also stated that "severe drought occurred with the Russian heat wave, making it likely that land surface feedbacks amplified this heat wave's intensity." Trenberth and Fasullo (2012), in contrast, linked the unusual anticyclone to the development of a large-scale Rossby wave train—suggesting that the wave train was forced by anomalous convection in the tropical Atlantic and northern Indian Oceans. They also argue that the heat wave intensified through the cumulative impact of local land feedbacks, linked to increased greenhouse gases. Lau and Kim (2012) highlighted the role of this wave train in linking the Russian heat wave to the Pakistani floods, with land feedbacks acting to amplify the Russian heat wave, and moisture transport from the Bay of Bengal (associated with the northward propagation of the monsoonal intraseasonal oscillation) helping to sustain and amplify the Pakistani rains. They argue that the western Russian blocking event was itself instrumental in forcing the Rossby wave. Galarneau et al. (2012) highlighted the importance of circulation around the blocking ridge accompanied by enhanced subsidence in the intensification of the heat wave. They also found that downstream energy dispersion from source regions over the North Atlantic modulated the structure and intensity of the blocking anticyclone over western Russia.

Schneidereit et al. (2012) argue that a number of factors at several different time scales were at work during the 2010 heat wave. They show that the shift to La Niña conditions modulated the stationary wave pattern, supporting the blocking high over eastern Europe. Also, they found that a polar Arctic dipole mode projected on the mean blocking high, and that transients acted to maintain it. At 10–60-day time scales they identified three different paths of wave action that also contributed to the persistent blocking conditions.

While numerous studies have addressed the important role of soil moisture feedbacks in European droughts (e.g., Ferranti and Viterbo 2006; Seneviratne et al. 2006; Fischer et al. 2007; Vautard et al. 2007; Zampieri et al. 2009; Stefanon et al. 2012), far fewer studies have focused on soil moisture impacts in the rest of Eurasia. Cherenkova

(2012) examined the precursors to summer drought in the European territory of Russia, finding that of the five most extensive hazardous droughts that occurred between 1936 and 2010 (1936, 1938, 1972, 1981, and 2010), three (1936, 1938, and 1972) were preceded by dry winters and springs, which created conditions for further drought development in the summer. The 1981 drought was not preceded by a dry winter and spring, and they suggest that this explains the smaller area covered by that drought. The 2010 drought was preceded by a cold winter without precipitation deficits, but they suggested that the cold temperatures did impact the snowmelt and spring soil moisture deficits. As already mentioned, Lau and Kim (2012) found that the 2010 Russian heat wave was amplified by the underlying extensive region of dry soil conditions.

Hirschi et al. (2011) examined the relationships among soil moisture, drought, and summer heat for central and southeastern Europe, based on observational indices for 275 station observations. They found that dry soil conditions intensified hot extremes in the southeastern (Romania and Bulgaria) area, especially for the high end of the distribution of temperature extremes, whereas this was not the case for central Europe (Austria and the Czech Republic); they further noted that while the former area is characterized by soil moisture–limited evaporation, the latter is characterized by energy-limited evaporation. Mueller and Seneviratne (2012) show that the dryness–temperature relationship is important in many areas of the world including much of eastern Europe (extending east into European Russia to about 50°E), where the probability of occurrence of an above-average number of hot days with preceding precipitation deficits is over 60%. Volodin (2011) analyzed the causes of "super-extreme" anomalies of summer surface air temperature in a suite of GCM experiments and reanalyses, focusing on the summer 2010 hot spell over ER as well as similar hot spells in western Europe (2003) and the contiguous United States (in 1980 and 2007). He showed that, in addition to the atmospheric factors acting during the peak month of drought (in the case of ER in July 2010 this was a prolonged atmospheric blocking event), preceding monthly anomalies of soil moisture located windward of the drought significantly enhanced the temperature anomaly. This behavior repeated itself over ER in the summer of 2012 where the drought (and the soil moisture anomaly) began initially over Kazakhstan and the southernmost areas of ER and gradually expanded northward. Lorenz et al. (2010) analyzed regional climate model simulations to show that soil moisture memory also acts to increase the persistence (in addition to the intensity) of heat wave events.

Koster et al. (2006b, see their Fig. 11) showed that the observed spatial pattern of interannual JJA temperature variance over North America can be reproduced by an AGCM only when soil moisture feedback processes are allowed to operate in the model, a strong indication that soil moisture variability contributes significantly to temperature variability. An analogous figure for Eurasia is shown here in Fig. 5. Figure 5a, from observations [Modern-Era Retrospective Analysis for Research and Applications (MERRA)], shows monthly temperature variance for the JJA period over 1980–2012. To first order, the free-running Goddard Earth Observing System, version 5 (GEOS-5), AGCM (Fig. 5b) reproduces this structure, with high variability in the most northern parts of Eurasia and another band of high variability centered at about 50°N. (The variances produced by the free-running model and MERRA differ mostly in their amplitudes, with weaker values seen in the former.) Figure 5c shows the temperature variances generated by the GEOS-5 AGCM when soil moisture feedback processes are artificially disabled, a condition achieved here by continually resetting the land model's soil moisture prognostic variables to seasonally varying climatological values (see appendix A). Disabling soil moisture feedback significantly reduces the variances along a swath through the center of the continent, extending from southern Europe eastward across the Caucasus to Kazakhstan, Mongolia, and northern China (Fig. 5d). This swath of reduction is indeed where we expect it to be, located at the transition between the wet climate to the north and the dry climate to the south; evaporation variance associated with soil moisture variations tends to be maximized in such a transition regime (see Koster et al. 2006b). In the AGCM, soil moisture feedback is unequivocally responsible for enhanced temperature variance along this swath, and we can speculate that the same is true in nature. We will come back to the role of the land later in our discussion of long-term trends and predictability.

The role of SST in seasonal to decadal climate variability over Eurasia is also still not well understood. Again, much of the analysis of the role of SST has focused on impacts in Europe, although a number of these studies have implications for regions to the east. Ionita et al. (2012) analyzed the self-calibrating Palmer drought index (van der Schrier et al. 2006) for the period 1901–2002 and found considerable interannual and multidecadal variability in summer moisture over Europe that was tied to SST variability. In addition to a drying trend over Europe associated with warming SST over all oceans, they found a link between previous winter La Niña and negative Pacific decadal oscillation (PDO) events and summer dry conditions over southern Europe extending into western Russia, and wet conditions over the Scandinavian peninsula, with the atmospheric anomalies resembling aspects

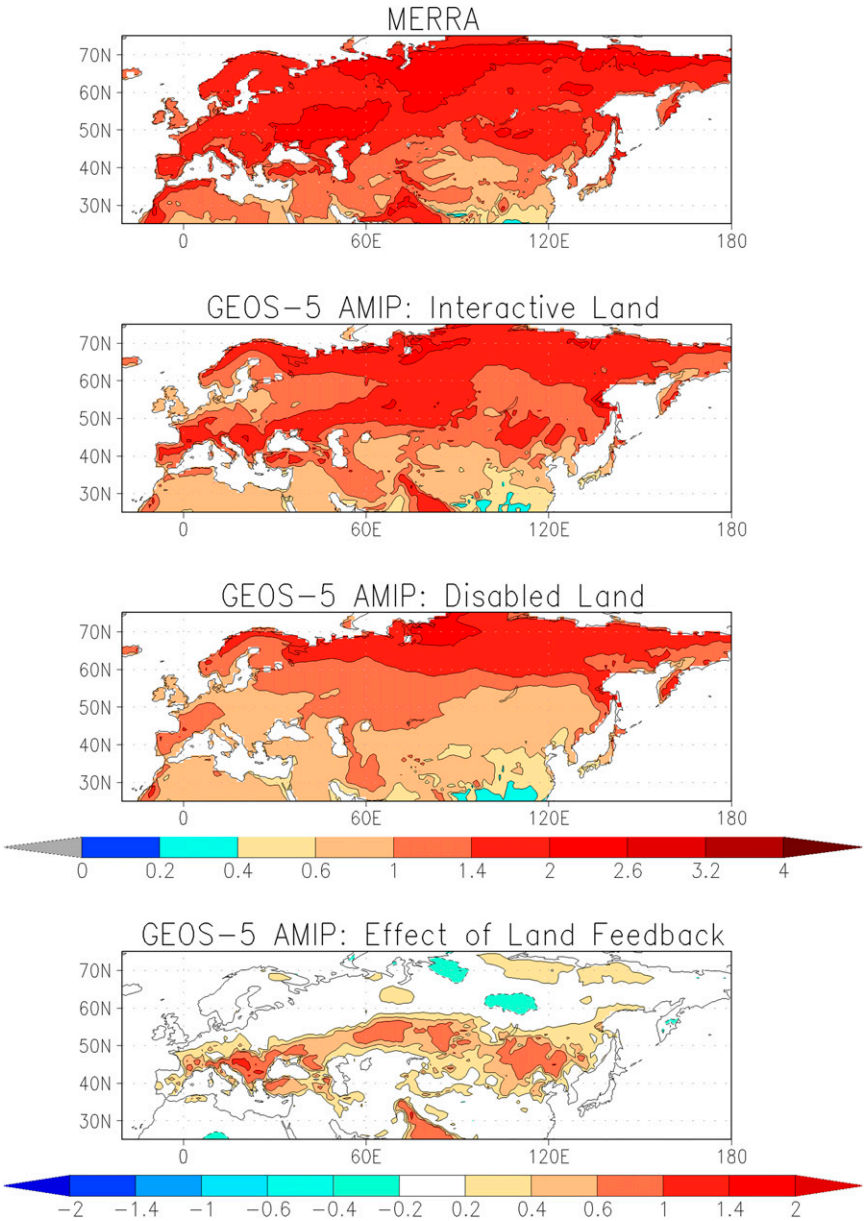

FIG. 5. The standard deviation of the monthly JJA 2-m temperature (°C) for the period 1980–2012: (top) MERRA, (second row) GEOS-5 AGCM simulations with interactive land, and (third row) GEOS-5 AGCM simulations with disabled land–atmosphere feedback. (bottom) The difference between the second row and the third row, indicating the effects of land–atmosphere feedback.

of the Pacific–North American pattern (PNA) and (the positive phase of) the North Atlantic Oscillation (NAO). They also found a link with the cold/negative phase of the Atlantic multidecadal oscillation (AMO) that leads to summer drought conditions extending across southern Scandinavia, southeastern Europe, and into northwestern Russia. They cite the extremely hot and dry summers of 1921 and 1972 over the central and northern regions of Russia (Buchinsky 1976) as examples of events that coincide with an AMO in its negative phase.

Sedláček et al. (2011) hypothesized that the SST anomalies in the Barents and the Arabian Seas combined to produce warming over Eurasia during 2010, thus contributing to the heat wave; they suggest that such a dynamic response to SST (in particular to the expected warming and reduction in sea ice over the Barents Sea)

will contribute to more frequent heat waves over Eurasia in the future. Wu et al. (2012) examined the impact of the NAO on the relationship between the East Asian summer monsoon and ENSO and found, among other things, that an anomalous spring NAO induces a tripole SST anomaly in the North Atlantic that persists into summer and excites downstream development of a Rossby wave train that modulates the blocking highs over the Ural Mountains and Okhotsk Sea. While the main impact of Arctic Sea ice reduction occurs during winter (Deser et al. 2007), a recent observational study by Francis and Vavrus (2012) suggests that the reduction in Arctic Sea ice slows the progression of Rossby waves by weakening the zonal winds and increasing wave amplitude. They argue that while these impacts are strongest during winter and autumn, they are also apparent in summer (possibly due to earlier snowmelt on high-latitude land) and therefore contribute to more extreme summer weather events including Eurasian heat waves.

b. *The role of stationary Rossby waves*

A recurring theme in the above discussion is the role of Rossby waves. Ambrizzi et al. (1995) provide one of the first studies to isolate the teleconnectivity associated with the boreal summer waveguides and preferred wave propagation patterns toward and away from the waveguides. Again, Schubert et al. (2011) identified a particular recurring Rossby wave (forced by submonthly vorticity transients) that extends across northern Eurasia and that contributes significantly to monthly surface temperature and precipitation variability, playing an important role in the generation of the 2003 European and 2010 Russian heat waves.

To the extent that Rossby waves are an important component of summer Eurasian temperature and precipitation variability, we would expect that the leading surface temperature and precipitation REOFs shown in Fig. 3 would be tied to such atmospheric waves. The correlations between the leading RPCs and the monthly 250-mb v wind (Fig. 6) suggest that this is indeed the case. The correlations with the first two RPCs show two clear wave structures that are approximately in quadrature extending across northern Eurasia. In fact these closely resemble the Schubert et al. (2011) basic wave structure of the leading REOF of the monthly 250-mb v wind mentioned above. The correlation pattern associated with the first RPC differs somewhat from that of the second in that the anomalies seem to extend around the globe, and there is a clear signature of a split in the wave over Europe with the northern component extending across Eurasia to the north of the mean jet, and a southern component that appears to use the mean jet as a waveguide (this correlation pattern is very similar to the actual 250-mb v-wind anomalies during July 2010; cf. Fig. 7). The correlations associated with the second RPC suggest a wave development that is more confined to the northern part of Eurasia (north of the mean jet) and resembles the June 2003 v-wind anomalies (Fig. 7).

The correlations with the third RPC (Fig. 6) show a wave structure that is more confined to the mean jet throughout the Northern Hemisphere; over Eurasia it appears to affect primarily southern Europe and the regions east of the Caspian Sea. This pattern dominates the v-wind anomalies, for example, in August 1992 (Fig. 7). The fourth and fifth RPCs are associated with wave structures similar to those of the other leading modes, but with that of the fourth having its largest amplitude over the eastern half of Eurasia (e.g., August 2001 in Fig. 7), and that of the fifth having its largest amplitude over northeast Atlantic and northern Europe (e.g., July 1994 in Fig. 7).

The potential role of SST anomalies in forcing the leading REOFs was examined by computing the simultaneous and time-lagged correlations with the global monthly SST anomalies (not shown). The results indicate that the correlations are generally weak (absolute values less than 0.3). An exception to that is RPC 1, which has somewhat larger negative correlations (between −0.3 and −0.4) in the tropical eastern Pacific at both 0 and −1 month lags, suggesting a weak link to ENSO. Also, RPC 3 has positive correlations with SST (between 0.3 and 0.4 at lag 0) over the North Atlantic, with a similar pattern of correlations (but weaker) occurring at −1 lag. The largest correlations with SST occur for RPC 5 (values greater than 0.5 at lag 0) over the far eastern North Atlantic and Mediterranean Sea in the immediate vicinity of Europe: these likely reflect the response of the SST to the changes in atmospheric forcing associated with the wave itself. The above results indicate that SSTs have only a weak (if any) impact on the development of these waves on monthly time scales, with perhaps ENSO and the North Atlantic SST having some influence on RPCs 1 and 3, respectively. An important caveat here is that the above correlations reflect primarily interannual linkages in the monthly statistics, rather than subseasonal linkages. In fact, if we remove the interannual component of the variability, the correlations with SST are even weaker for all RPCs except for the simultaneous correlations associated with RPC 5 in the vicinity of Europe.

The forcing of such waves by submonthly vorticity transients is illustrated in Fig. 8 in the context of a stationary wave model (SWM; Ting and Yu 1998) forced by an idealized localized vorticity source in the North Atlantic jet exit region (see Schubert et al. 2011 for details). The results show that an atmospheric wave structure very similar to that associated with REOF 1 develops in

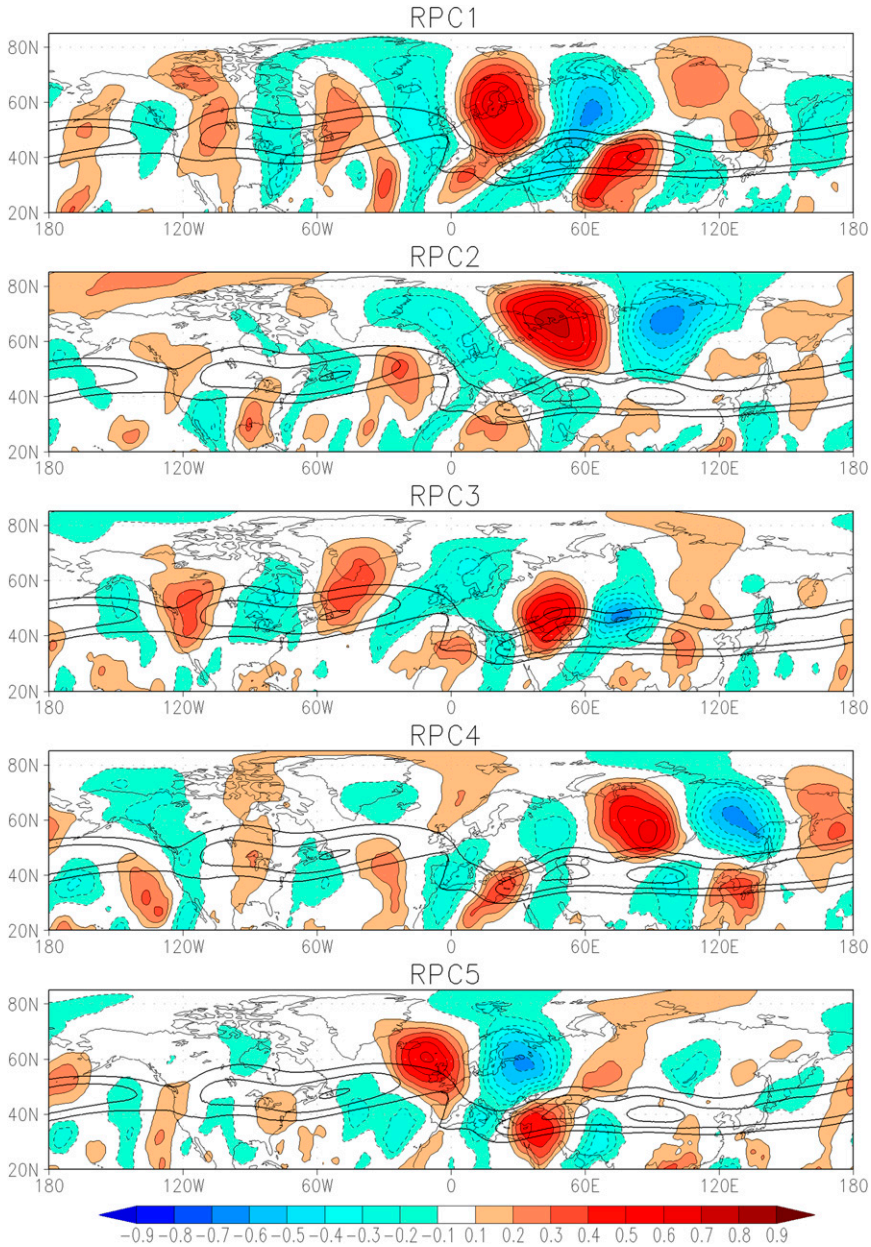

FIG. 6. The temporal correlation (shading) between the monthly JJA 250-mb meridional wind (v) and leading RPCs of combined 2-m temperature and precipitation for the period 1979–2012. A linear trend was removed for each calendar month before computing the covariances. Contours are the long-term mean JJA zonal wind (u) at 250 mb (15, 20, and 25 m s^{-1}). Results are for MERRA.

the SWM within about three weeks. While such Rossby waves (driven by internal atmospheric dynamics) appear to be a ubiquitous component of summertime weekly to monthly atmospheric variability over Eurasia, the mechanisms that lead to their occasional persistence and amplification are as yet unclear. An assessment of the potential role of soil moisture and a further assessment of SST forcing will be made in the following two sections, where we examine longer-term (from seasonal to decadal) variations and the predictability of such extreme events.

4. Past long-term behavior and trends

a. A review

The 2003 European and 2010 Russian heat waves, in addition to prompting numerous papers on causes and

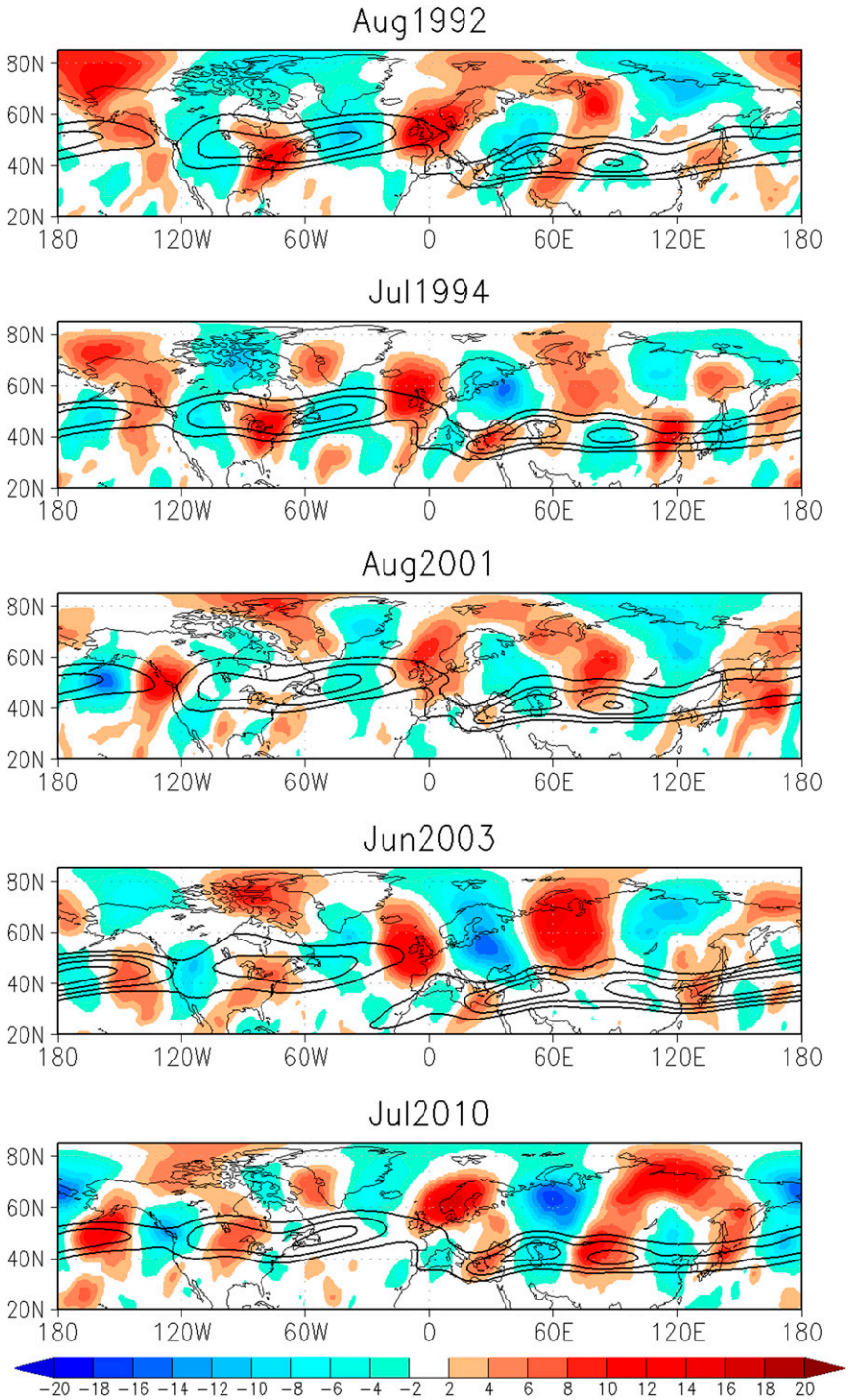

FIG. 7. Examples from MERRA of the 250-mb v-wind anomalies (with respect to the 1980–2010 climatology; $\mathrm{m\,s^{-1}}$) for selected months to highlight the predilection for Rossby wave structures similar to those shown in Fig. 6 that are linked to monthly variability in surface meteorology.

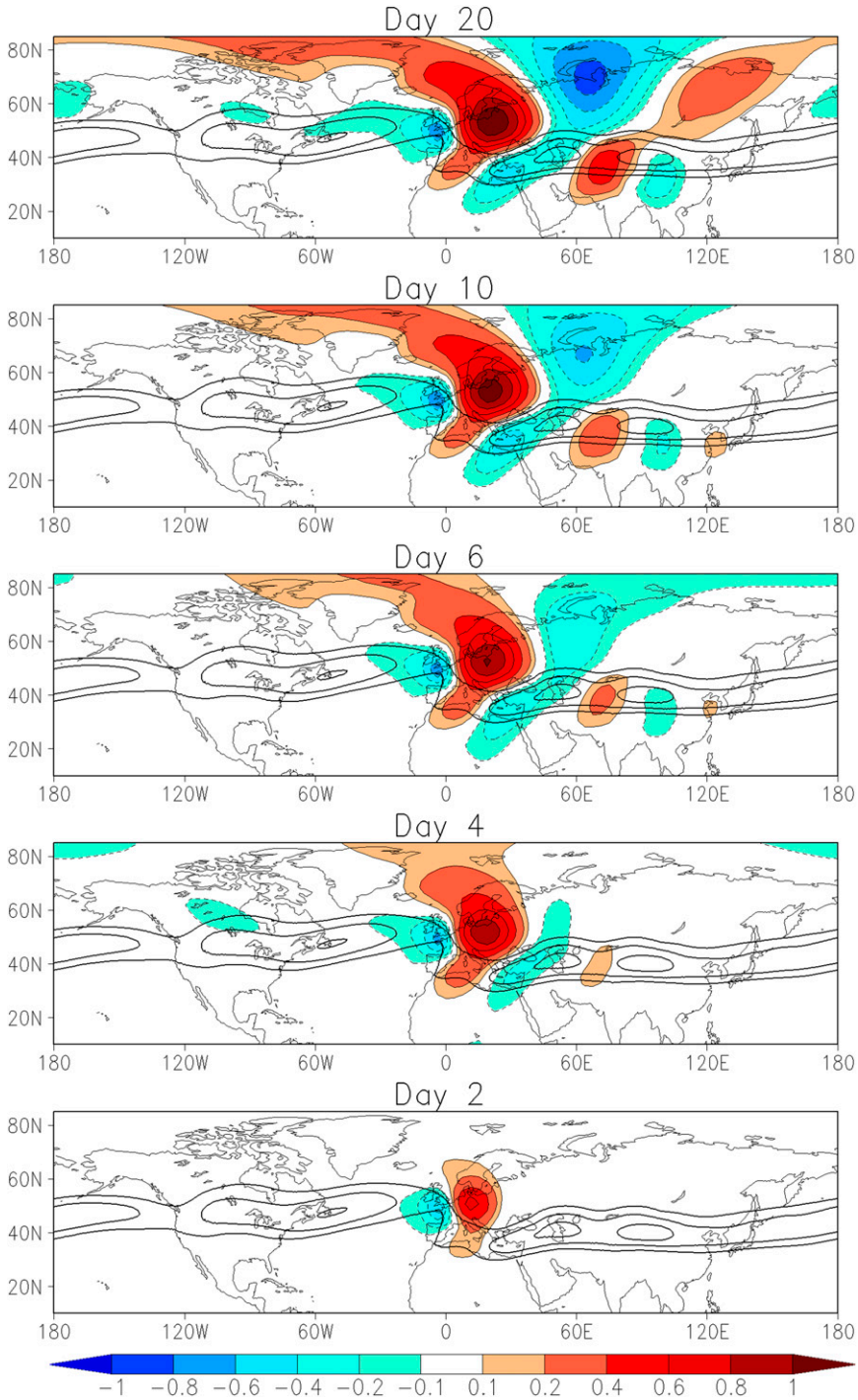

FIG. 8. The time evolution of the response of the eddy v-wind at $\sigma = 0.257$ to an idealized constant vorticity source at 50°N, 0°E. The results are from a stationary wave model (Ting and Yu 1998) with a three-dimensional JJA mean base state taken from MERRA for the period 1979–2010. The horizontal structure of the idealized forcing has a sine-squared functional form, with horizontal scales of 10° lat × 10° lon and vertical profile (maximum of $5.6 \times e^{-10}\,\mathrm{s}^{-1}$ in the upper troposphere) following Liu et al. (1998). See Schubert et al. (2011) for additional results. Contours are the long-term mean JJA zonal wind (u) at 250 mb (15, 20, and 25 m s^{-1}) from MERRA.

impacts, highlighted the ongoing debate about whether such events are early manifestations of global warming. For example, Rahmstorf and Coumou (2011), employing a stochastic model to examine the effect of warming trends on heat records, concluded that, with a probability of 80%, ''the 2010 July heat record would not have occurred'' without the large-scale climate warming seen since 1980, most of which has been attributed to the anthropogenic increase in greenhouse gas concentrations. In contrast, as already mentioned, Dole et al. (2011) conclude from their analysis of dynamical mechanisms that neither human influences nor slowly varying ocean boundary conditions contributed substantially to the magnitude of the 2010 event. Otto et al. (2012) examined the results from a large ensemble of atmospheric general circulation model simulations and concluded that ''there is no substantive contradiction between these two papers, in that the same event can be both mostly internally generated in terms of magnitude and mostly externally driven in terms of occurrence probability. The difference in conclusion between these two papers illustrates the importance of specifying precisely what question is being asked in addressing the issue of attribution of individual weather events to external drivers of climate.''

In addition to the current debate on whether the nature of extreme events is changing, there is also ongoing debate about basic trends in both the mean precipitation and surface temperature. Meshcherskaya and Blazhevich (1997) used station data to study changes in drought over the European and Asian parts of the former Soviet Union (FSU) for the period 1891–1995. They found that trends in their drought and excessive moisture index (DM, for May–July) are statistically significant only in the Asian part of the FSU and that the increased dryness is largely the result of temperature increases, with a small but statistically significant contribution coming from a decrease in precipitation. These results have recently been updated and expanded by Groisman et al. (2013), who showed that while heavy rainfall frequencies have increased in the past two decades, mean precipitation has grown more slowly or has even decreased, with an accompanying increase in the frequency of no-rain periods over most of northern Eurasia south of 60°N.

Alexander et al. (2006), using updated station data from the more recent record (1951–2003), examined a number of climate indices (see also Frich et al. 2002) and found significant changes in extremes associated with warming. In particular, they found that much of Eurasia is characterized by a significant decrease in the annual number of cold nights and an increase in the number of warm nights. These results hold for all seasons, with the largest changes occurring during March–May (MAM) and the smallest during September–November (SON). Corresponding behavior is also seen in a subset of stations with records going back to 1901. Precipitation indices show a tendency toward wetter conditions throughout the twentieth century.

Frey and Smith (2003) examined precipitation and temperature trends in station observations from western Siberia, a region with a large percentage of the world's peatlands, and one that contributes substantially to the terrestrial freshwater flux into the Arctic Sea. They found robust patterns of springtime warming and wintertime precipitation increases, with the Arctic Oscillation (AO) playing an important role in nonsummer warming trends. As noted by Folland et al. (2001), the AO (and NAO) had been in phase since the 1970s, producing enhanced westerlies and extratropical cold season warming across much of Eurasia.

Batima et al. (2005) examined data from 60 meteo-stations spanning Mongolia for the period 1940–2001 and found that the mean annual surface temperature has risen by 1.66°C over the 62-yr period, warming faster in winter than summer. The warming is more pronounced in mountainous areas and their valleys and is less pronounced in the Gobi desert. They also find a statistically insignificant decrease in annual mean precipitation, with winter and spring showing a decrease but summer and fall showing no change. Even without clear evidence for an increase in summer temperatures, summer heat wave duration has increased by 8–18 days, depending on location. The warmest year of the last century was 1998, and Mongolia experienced drought for the next four years (1999–2002). Batima et al. (2005) further note that the intense drought spells in recent years are most likely the result of both increased temperature and decreased precipitation. They emphasize that the environment and climate play a key role in the sustainability of Mongolia—animal husbandry employs 47.9% of the total population, producing 34.6% of the agricultural gross production and accounting for 30% of the country's exports. Nandintsetseg et al. (2007) found an almost 2°C increase in temperature in northern Mongolia between 1963 and 2002, along with a significant increase in warm extremes and a decrease in cold extremes. On average, they found neither a significant decrease in the maximum number of consecutive dry days nor an increase in the number of wet days.

Robock et al. (2005) examined 45 years (1958–2002) of soil moisture observations over Ukraine and found an increase in soil moisture over those years, despite a slight warming and a decrease in precipitation. They suggested that this is the result of increased aerosols in the troposphere leading to decreased solar insolation, which acts to reduce evaporation; the reduced evaporation in turn leads to increased surface temperature and soil moisture.

Parry et al. (2007, see Table 10.2 therein) summarize some of the key trends in northern Eurasia, with Russia experiencing a 2°–3°C rise in the past 90 years that is most pronounced in spring and winter. Changes in precipitation in Russia are highly variable with a decrease during 1951–95 and an increase in the last decade. Central Asia experienced a 1°–2°C rise in temperature per century, with no clear trend in precipitation between 1900 and 1996. Mongolia has seen a 1.8°C increase in the last 60 years that is most pronounced in winter; Mongolian precipitation has decreased by 7.5% in summer and has increased by 9% in winter.

Analyses covering longer time periods are also available. Briffa et al. (1995) report on a 1000-yr tree-ring reconstruction of summer temperatures over the northern Urals; they show that the mean temperature of the twentieth century is higher than that of any other century since AD 914. Demezhko and Golovanova (2007) reconstructed ground surface temperatures from AD 800 onward based on borehole temperature logs and 170 years of meteorological data over the southern and eastern Urals. They conclude that the mean temperature during the medieval maximum (AD 1100–1200) was 0.4 K higher than that for the period 1900–60. They also conclude that cooling during the ''Little Ice Age'' culminated in about AD 1720 with a mean surface temperature 1.6°C below the 1900–60 mean, and they note that the contemporary warming began about a century prior to the first instrumental records in the Urals, with the mean rate of warming increasing in the final decades of the twentieth century.

The recent special report of the Intergovernmental Panel on Climate Change (IPCC) on extremes (Field et al. 2012) provides an updated summary of the current confidence placed in recent trends of heat waves and droughts. The report notes that in Asia there is ''overall low confidence in trends in dryness both at the continental and regional scale, mostly due to spatially varying trends, except in East Asia where a range of studies, based on different indices, show increasing dryness in the second half of the 20th century, leading to medium confidence.'' They also note that since 1950, there is medium confidence in a warming trend in daily temperature extremes over much of Asia.

b. *A model-based analysis of recent trends (1979–2012)*

In this section, we utilize numerical simulations to provide further insight into the nature of recent variability and trends over Eurasia. These simulations take the form of full global reanalyses [MERRA and the Interim European Centre for Medium-Range Weather Forecasts (ECMWF) Re-Analysis (ERA-Interim)], Atmospheric Model Intercomparison Project (AMIP)-style simulations using the Global Modeling and Assimilation Office (GMAO) GEOS-5 system, and simulations with more idealized SST forcing.

One of the intriguing aspects of RPC 1 in Fig. 4 is the apparent trend or shift in the time series from being predominantly negative prior to about 1995 to predominantly positive thereafter. There is an indication of a similar shift in RPCs 3 and 4. The first three panels on the left of Fig. 9 (derived from the two reanalyses and from station observations) indicate that these shifts appear to be part of a hemispheric-wide pattern of warming over the last three decades, with the maxima over Eurasia centered over European Russia and Mongolia/eastern Siberia. While the maps from the reanalyses differ somewhat from that constructed with the station observations, especially regarding the amplitude of the changes, overall they agree on the main regions of warming. As for precipitation (the first three panels on the right side of Fig. 9), the patterns of change are more complex, with decreases covering parts of northeastern Europe, European Russia, Kazakhstan, southeastern Siberia, Mongolia, and northern China, and with increases found across Siberia north of about 60°N.

The extent to which the above trends are a reflection of global warming and/or the result of other long-term (decadal) variability is still an open question. Some insight into this issue can be gained from the analysis of free-running climate model simulations. We examine now an ensemble of 12 GEOS-5 AMIP simulations driven by observed SST and greenhouse gas (GHG) forcing over the period from 1871 to the present. The 1996–2011 minus 1980–95 differences for the ensemble mean are shown in the bottom panels of Fig. 9. Overall the model results are consistent with the reanalyses and observations, showing warming over basically the same regions across Eurasia (southern Europe and European Russia, Kazakhstan/southern Siberia, Mongolia, and northern China), although with weaker amplitude. We note, however, that individual ensemble members (not shown) exhibit changes as large as the observed and that there is substantial intraensemble variability in the detailed spatial patterns of the differences, with some showing the same two-lobed structure found in the observations. The model ensemble mean also reproduces to some degree the overall pattern of precipitation changes (although again with weaker amplitude than observed), including the tendency for precipitation deficits over European Russia and over Siberia south of about 60°N, and for precipitation increases to the north.

The AMIP results in Fig. 9 suggest that SST variations and perhaps the direct GHG forcing are contributing significantly to the observed JJA trends in Eurasian

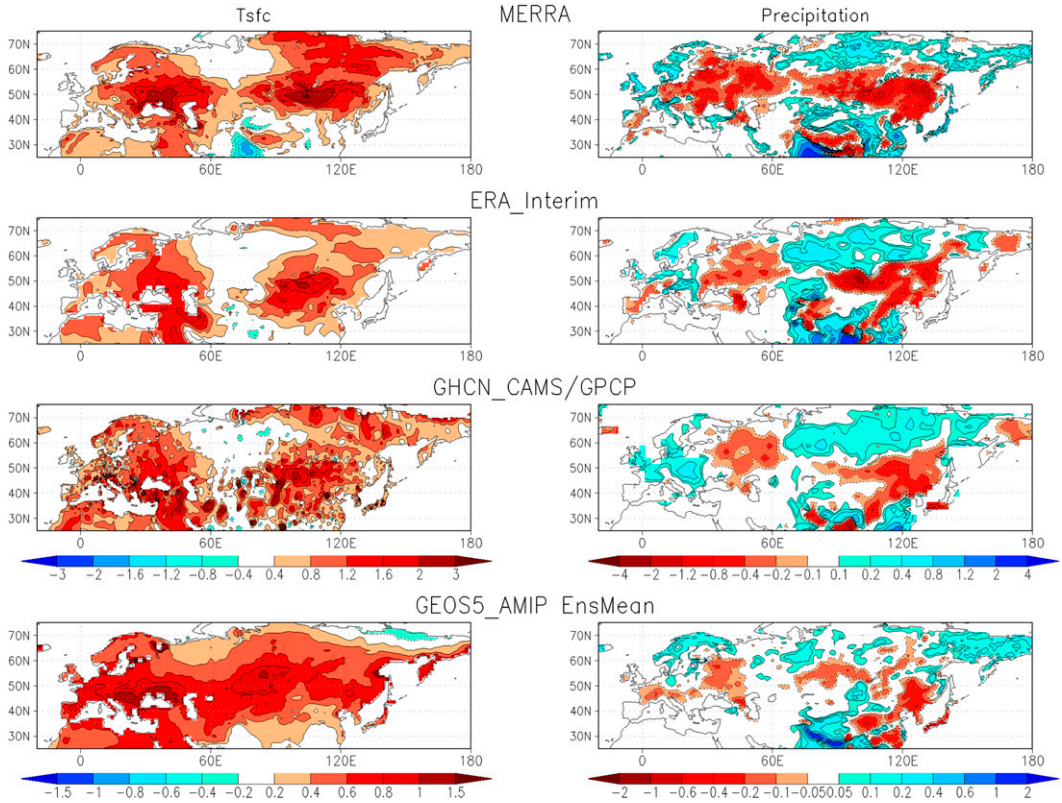

FIG. 9. The difference between the long-term JJA means (1996–2011 minus 1980–95) for (left) 2-m temperature (°C) and (right) precipitation (mm day^{-1}), for (top) MERRA, (second row) ERA-Interim, (third row) GHCN_CAMS (for 2-m temperature) and GPCP (for precipitation), and (bottom) the ensemble mean of the AMIP runs. Note the different shading intervals for the ensemble means.

surface temperature and precipitation seen over the last three decades. Figure 10 (left panel) shows the linear trend in observed SST during that period (1980–2011). The SST trend pattern shows aspects of overall warming combined with a La Niña–like pattern in the Pacific and a positive AMO pattern in the Atlantic. This is compared (right panel of Fig. 10) with one of the idealized SST forcing patterns used recently by the U.S. Climate Variability and Predictability (CLIVAR) Drought Working group to force several different climate models (Schubert et al. 2009). This latter pattern is the sum of the three leading REOFs of annual mean SST, consisting of a PDO/La Niña–like pattern, an AMO-like pattern, and the warming trend pattern. With the exception of the Indian Ocean, the similarity of this idealized pattern to the recent (three decade long) trend pattern is striking, suggesting that the recent trends are a mixture of both decadal variability and long-term trends.

Figure 11 shows, for the average of three of the models that participated in the U.S. CLIVAR drought working group project (Schubert et al. 2009) and GEOS-5, the JJA surface temperature response to the idealized SST pattern shown in the right panel of Fig. 10. The results are based on 50-yr-long simulations for all the models except the Climate Forecast System (CFS), which was integrated for 35 yr. The models produce warming (top left panel) over most of Eurasia between 30° and 60°N. The precipitation anomalies (top right) consist of deficits over central Eurasia (centered on about 50°N, 95°E) and parts of Europe. Positive precipitation anomalies occur over much of the northern regions of Russia, especially east of about 70°E, extending into northeastern China. Additional runs with these models (not shown) indicate that the Pacific and Atlantic SST patterns act to focus the warming and precipitation deficits in the midlatitude band between 30° and 60°N, as well as to produce some regional (east–west) variations that differ from model to model. The SST trend pattern acts to expand and enhance the regions of warming, with an overall tendency to warm the continents everywhere.[7] These

[7] There are some regions of cooling over land in response to the SST trend pattern (which itself has some spatial variability), although these tend to be relatively small in area and have small amplitude of cooling.

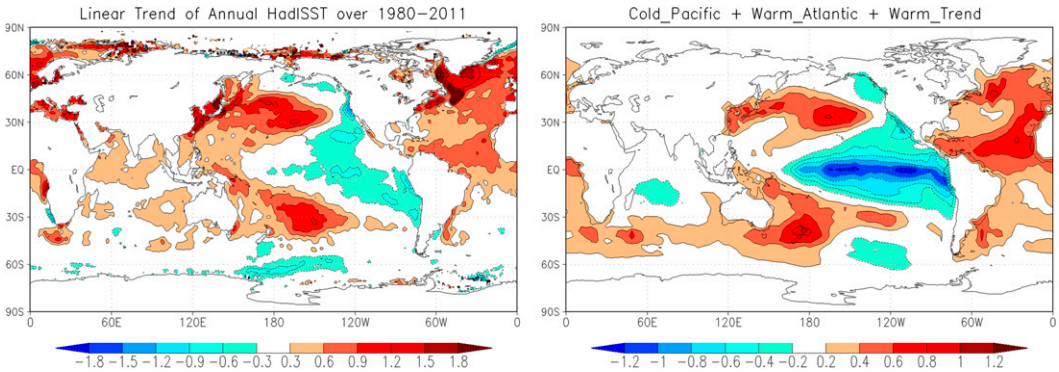

FIG. 10. (left) The linear trend in the annual mean SST from Hadley Centre Global Sea Ice and Sea Surface Temperature (HadISST), version 1, (Rayner et al. 2003) for the period 1980–2011. (right) The idealized SST forcing pattern that was used in the U.S. CLIVAR drought working group to force various climate models. The pattern is composed of the three leading REOFs of the annual mean SST consisting of the cold phase of a Pacific decadal mode, the warm phase of an Atlantic multidecadal oscillation (AMO)-like mode, and the trend pattern (see Schubert et al. 2009).

results are generally consistent with those shown in Fig. 9, supporting the idea that the main features of the northern Eurasian precipitation and temperature trends of the last three decades are largely forced by the leading patterns of SST variability (the global trend and the two dominant patterns of SST variability in the Pacific and Atlantic Oceans). The bottom panel of Fig. 11 suggests that the surface warming and precipitation changes are linked to a tendency for all the models to produce a band of positive upper tropospheric height anomalies throughout the midlatitudes of both hemispheres in response to the imposed SST patterns, and that (as shown by additional runs isolating the SST trend impacts; not shown) these positive height anomalies, while basically forced by the Pacific and Atlantic SST patterns, are amplified with the additional forcing of the SST trend pattern.

c. *An analysis of long-term variability (1871–2010)*

To put the trends of the last three decades in perspective, we now turn to temperature records going back to the late nineteenth century. The left panels in Fig. 12 show the time series of JJA mean temperature for the period 1871–2010, based on version 4 of the Climate Research Unit temperature database (CRUTEM4),

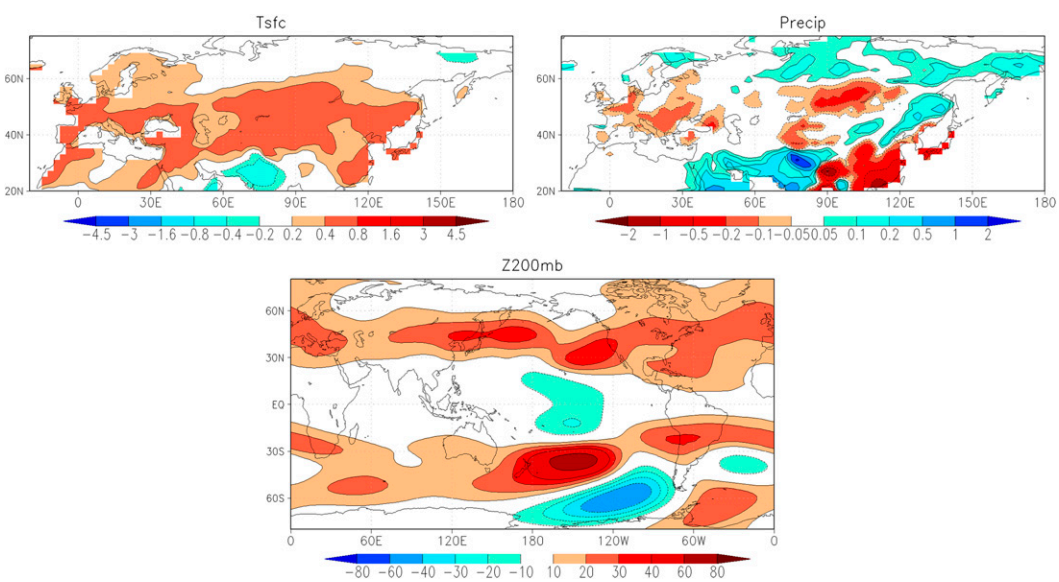

FIG. 11. The JJA responses to the idealized SST forcing pattern shown in the right panel of Fig. 10 averaged over four different AGCMs [Community Climate Model, version 3 (CCM3), GEOS-5, GFS, and Geophysical Fluid Dynamics Laboratory (GFDL) model]: (top left) surface temperature (°C), (top right) precipitation (mm day^{-1}), and (bottom) 200-mb height (m).

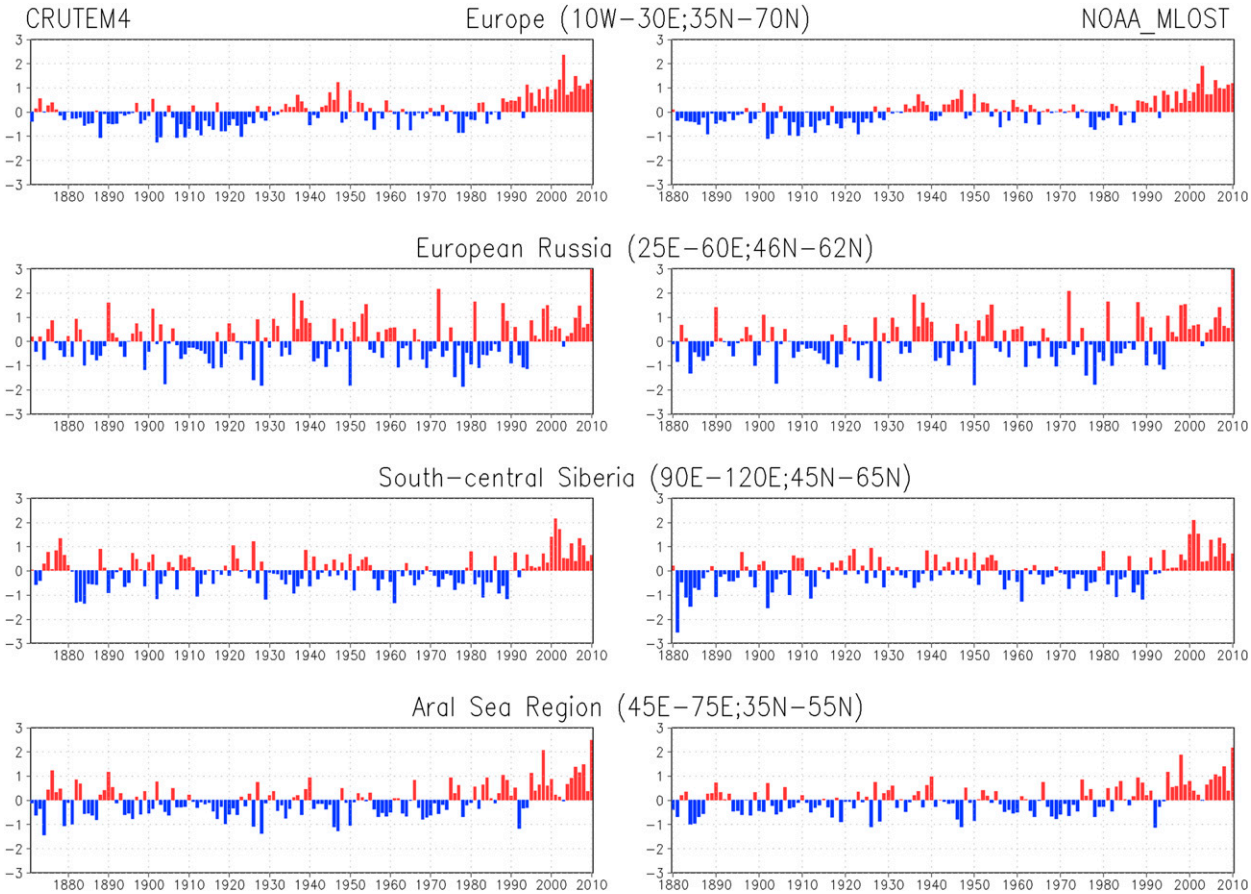

FIG. 12. The time series of the 2-m temperature anomalies (°C) for four different regions across Eurasia: (top) Europe (35°–70°N, 10°W–30°E); (second row) European Russia (46°–62°N, 25°–60°E); (third row) south-central Siberia (45°–65°N, 90°–120°E); and (bottom) Aral Sea region (35°–55°N, 45°–75°E), based on (left) CRUTEM4 data (1871–2010) and (right) NOAA MLOST data (1880–2010).

for four different regions in northern Eurasia: Europe, European Russia, south-central Siberia, and a cold desert region just east of the Caspian Sea, centered on the Aral Sea. (The definition of the regions was guided by the regions of maximum 2-m temperature loadings of the leading REOFs shown in Fig. 3.) All four regions show predominantly positive anomalies beginning shortly after 1990, although this is most pronounced for the European region. The 2010 heat wave stands out in the European Russia time series, although there are some other years with large anomalies, including 1972 (during the ''100-year'' drought; see also appendix B). While there is substantial interannual- and decadal-scale variability in all of the time series, there is also evidence of a long-term positive trend, although the trend values appear to depend somewhat on the observations during the late nineteenth century, which are likely not very reliable in the CRUTEM4 dataset. This is illustrated through comparison with another dataset [the National Oceanic and Atmospheric Administration (NOAA) Merged Land-Ocean Surface Temperature Analysis (MLOST); right panels of Fig. 12], indicating some differences during the early years, especially for the more eastern region. The latter dataset shows clearer long-term trends in part because it does not include the 1870s, which in the CRUTEM4 data is a period of positive anomalies. Note that extensive *standard* surface air temperature observations over the Russian Empire territory began in 1881 (Vannari 1911).

Figure 13 is the same as Fig. 12, but constructed from the output of two representative members of the aforementioned 12-member ensemble of 140-yr AMIP simulations with GEOS-5 (see appendix A). Each time series shows a basic character that is remarkably similar to that of the observations, with a shift toward positive anomalies starting in the 1990s. The long-term trend in all four regions is, in fact, even more pronounced in the model simulations. The simulations also show a few very extreme anomalies. In particular, we point out the unusually large positive (+3°C) anomaly simulated in 2001

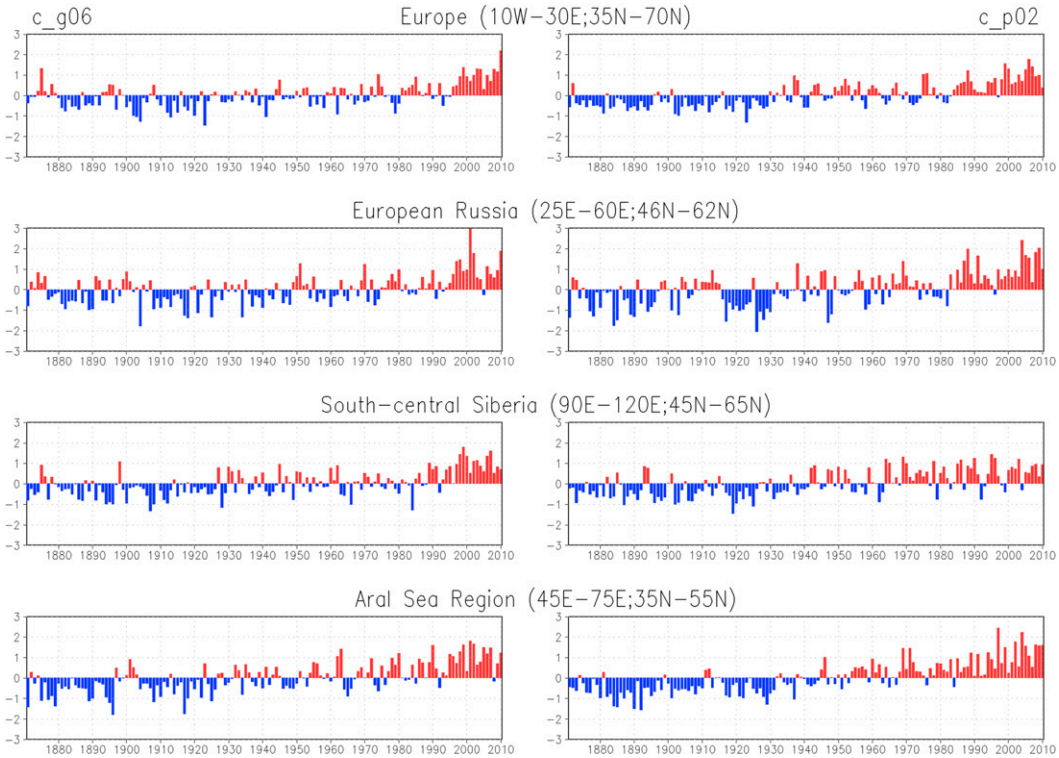

FIG. 13. As in Fig. 12, but for two of the 12 ensemble members of the GEOS-5 AGCM simulations forced with observed SST and GHG forcings for the period 1871–2010.

in European Russia in one of the ensemble members (second row of Fig. 13, on left). This event has a temperature signal comparable in magnitude to that observed during the 2010 Russian heat wave (Fig. 12) and will be examined in more detail in the next section. We note that similar events (temperature anomalies near +3°C) occur in some of the other ensemble members, although in general they are quite rare and are limited to the recent decades (e.g., there were only three such events in Europe and only two in European Russia in the entire ensemble of 12 runs, i.e., over a span of 1680 simulation years).

We next examine whether the interannual JJA mean surface temperature (T_s) variations in these regions are linked to SST variability. Figure 14 shows the temporal correlations of the regional mean T_s for the European Russia region with T_s values everywhere across the globe (using SST over the oceans). The calculation is limited to the years 1901–80 in order to avoid the earliest years with little observational data and to avoid the three most recent decades, which show the shift toward positive values. In addition, a linear trend was removed from all time series prior to computing the correlations. The results for the observations (top panel)—absolute values greater than 0.22 are significant at the 0.05% level (see www.mtsu.edu/~dwalsh/436/CORRSIG.pdf)—show a wave structure over northern Eurasia that is very similar to the leading REOF of the monthly data for the recent three decades (Fig. 3 top-left panel), suggesting that the seasonal data also project onto a Rossby wave structure, consistent with the findings of Schubert et al. (2011). There are also positive correlations over the Atlantic and the eastern Pacific, suggesting some link to the SST. The results for the model are shown in the middle and bottom panels of Fig. 14. The middle panel shows the correlations computed separately for each ensemble member and then averaged over the 12 ensemble members—a result that is more comparable to the correlations based on the observations. The model results clearly show the same basic wave structure of the correlations over northern Eurasia. By this measure, the link to the oceans is weak, with only small positive correlations (0.1–0.2) that are mainly confined to the Atlantic; however, there are individual ensemble members (not shown) that have correlations resembling those based on the observations (highlighting a considerable unforced component to the observational results). The bottom panel in Fig. 14 shows the correlations with the ensemble mean T_s. This calculation isolates the impact of the forcing common to all the ensemble members (SST and GHGs), showing, for example, correlations over the North Atlantic that exceed 0.4. Also, it is noteworthy that the pattern of correlations

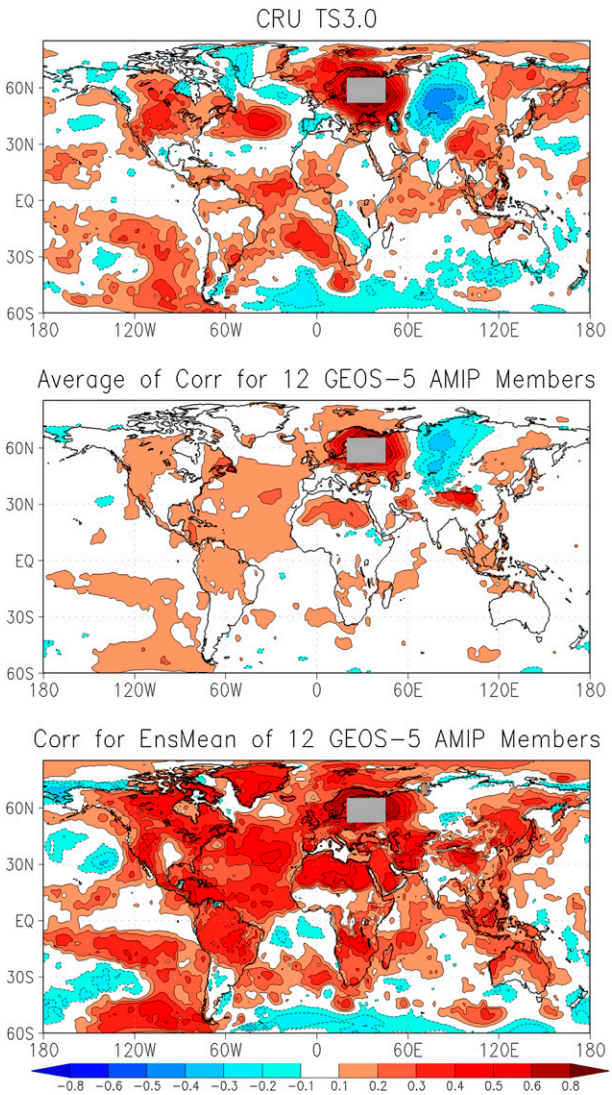

FIG. 14. The correlation between the JJA mean surface temperature averaged over European Russia (52°–65°N, 20°–45°E, indicated by the box), and the surface temperature everywhere for the period 1901–80. All data have a linear trend removed at each grid point before computing the correlations. (top) The CRU TS3.0 observations and (middle) the 12 GEOS-5 AMIP simulations. Here the correlations are computed for each ensemble member separately and then the correlations are averaged. (bottom) The 12 AMIP simulations, but here the correlations are based on the ensemble mean.

over the eastern Pacific is very similar to that based on the observations. Other regions with relatively large correlations include northern Africa, southern Eurasia, Canada, and the western United States. Further analysis (not shown) indicates that the patterns of the correlations are quite sensitive to the location of the target area. Analogous global maps of T_s correlations with T_s values in southern Europe, for example, show substantial negative correlations in the tropical Pacific and the Indian Ocean (for the ensemble mean), as well as positive correlations with the North Atlantic SST; the spatial pattern of these correlations over the ocean indeed resembles the spatial pattern of the SST anomalies shown in Fig. 10.

In summary, there appear to be significant temporal correlations between JJA surface temperature over large regions of Eurasia and SST, particularly in the North Atlantic and the tropical Pacific. However, the SST-forced response appears to be intertwined with and sensitive to the excitation of the basic internally generated Rossby wave structures discussed previously. This aspect of the response is currently not well understood.

5. Predictability and projections

In this section we review and provide new results on the predictability of drought and heat waves. We also review studies that examine longer-term projections, including those that examine overall trends in precipitation and temperature and provide an outlook for future heat waves and droughts.

a. A review of predictability

The predictability of heat waves and associated droughts is particularly challenging in view of their strong link to the development of persistent anticyclones, blocking, and stationary Rossby waves (see previous section on mechanisms). Most weather and climate models do not adequately represent blocking events (e.g., Scaife et al. 2010); they underestimate the occurrence of blocking as well as its intensity and duration. In addition, the basic predictability of blocking is likely rather short (perhaps a few weeks), since blocking ridges are believed to be maintained by interactions with smaller-scale weather systems (e.g., Scaife et al. 2010). The aforementioned results tying the development of major Eurasian heat waves to stationary Rossby waves also indicates relatively short predictability time scales, since the main forcing of such waves appears to be submonthly weather transients (e.g., Schubert et al. 2011). We note that the link between Rossby waves and the development of blocking events is still unclear (e.g., Nascimento and Ambrizzi 2002; Woollings et al. 2008).

Soil moisture anomalies and associated land–atmosphere feedbacks do provide some hope for skillful predictions out to perhaps 2 months (i.e., beyond weather time scales), although the levels of attainable skill, particularly given the observational networks available for soil moisture initialization, are modest at best (Koster et al. 2011; see also Volodin 2011). As discussed above, it is still an open question whether links to SST variability are sufficiently robust to provide useful forecast skill at

seasonal to interannual time scales, though there is some evidence that Arctic sea ice changes could provide some predictable signals. Modes of variability such as the NAO, NAM, and the East Atlantic/western Russia and Scandinavian modes, while primarily associated with cold season variability, can also play a role by preconditioning the soil moisture for the subsequent summer. While the NAO appears to have limited predictability on monthly and longer time scales (e.g., Johansson 2007), being largely driven by internal atmospheric dynamics, some evidence suggests that predictability may be provided through the coupling of the NAM with the stratosphere (e.g., Körnich 2010). Basic understanding of the mechanisms and predictability of the EA/WR and Scandinavian modes is not well understood. Monsoonal flows (e.g., Trenberth and Fasullo 2012) provide another potential source of predictability, although the current capability of simulating Asian monsoon variability is quite limited.

The 2010 heat wave provides an important example of our current ability to predict a particularly extreme event. Matsueda (2011), using medium-range ensemble forecasts, showed some success in predicting aspects of the blocking and extreme surface temperatures associated with the event out to a lead time of 9 days, although the later stages of the blocking in early August were less well predicted, with most models predicting a too early decay of the blocking. Ghelli et al. (2011) found signs of the developing heat wave about 3 weeks in advance in predictions with ECMWF's suite of models, although the full amplitude of the event was not predicted until about 1 week in advance. These results are consistent with the study by Dole et al. (2011), which found no change in the probability of prolonged blocking events over western Russia during July 2010 for forecasts initialized in early June of that year, compared with hindcasts initialized in early June of other years (1981–2008).

b. A case study

Here, using a more idealized approach, we present new results concerning the basic predictability of extreme heat waves and associated drought events. We examine the predictability of one of the most extreme events to occur over European Russia in our multidecadal GEOS-5 AMIP simulations: the extreme heat event simulated by one of our ensemble members in the summer of 2001 (see discussion of Fig. 13). We remind the reader that the fact that this event happened to occur in 2001 in the simulation (rather than 2010 as in nature) appears to be purely by chance, since there is no consistency among the various ensemble members as to the timing of such events. Here we chose the event that occurred in 2001 in ensemble member 6 because it was one of the most extreme simulated events to occur over basically the same region as the observed event of 2010. Figure 15 shows the evolution of the surface air temperature, upper tropospheric meridional wind, and soil moisture from May through August of that year. The surface air temperature anomalies during May show a wave structure across northern Eurasia, the same structure that characterizes the monthly variability of observations (e.g., Fig. 3). At this time the largest temperature anomalies occur over eastern Siberia, with negative anomalies to the west and positive anomalies over eastern Europe and European Russia. The same basic structure continues into June, showing some propagation to the east and intensification of the warm anomalies over European Russia, especially just north of the Black Sea, where it achieves its maximum amplitude of more than 5°C. By July the wave structure is more diffuse, but the warm anomalies over European Russia continue through July and well into August. The upper-level wind shows that the T_s anomalies are associated with Rossby wave–like structures that develop in May, peak in June, and dissipate thereafter. The soil moisture anomalies show the same basic wave structure, though somewhat phase shifted to the east of the temperature anomalies. The negative soil moisture anomalies over European Russia are already evident in May (just north of the Black and Caspian Seas), intensifying in June and continuing through July into August. As the T_s anomalies move to the east, they appear to become phase locked with the soil moisture anomalies beginning with July and extending into August.

Our interpretation of the above results is that the heat wave was initiated by the development of a Rossby wave (May and June). This wave generated T_s anomalies that eventually became phase locked with existing dry soil moisture anomalies over European Russia, which acted to intensify and persist the T_s anomalies beyond the lifespan of the Rossby wave. We note that central ER (specifically the region 50°–60°N, 30°–48°E) in that ensemble member experienced soil moisture deficits for almost a decade from the mid-1990s to early 2003, deficits that appear to be part of a general drying and warming trend (evident also in the ensemble mean) that begins in the mid-twentieth century and becomes especially pronounced after the mid-1990s. This suggests that the SST/GHG forcing may have set the stage for the development of the extremely warm summer over European Russia. We note that the evolution described here is quite similar to that found in Lyon and Dole (1995) for the 1980 and 1988 U.S. drought cases, where anomalous wave trains associated with early stages of heat wave/droughts became very weak by early July, with reductions in evapotranspiration over the drought

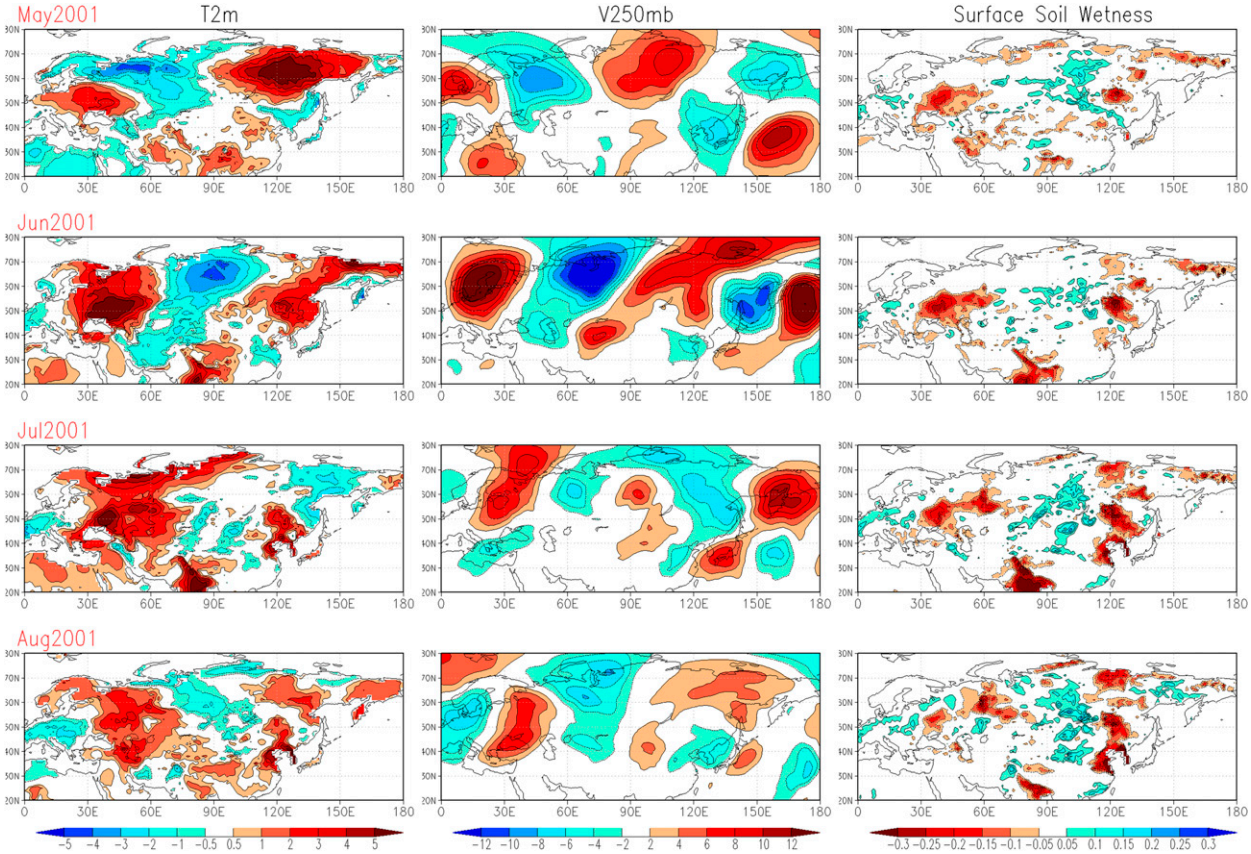

FIG. 15. Results from one of the most extreme heat waves in European Russia found in the GEOS-5 AGCM simulations (see text for details). (left) The evolution of the 2-m temperature anomalies (°C) from the simulation for May–August 2001 (anomalies are computed with respect to the 1980–2010 mean). (center) The evolution of the 250-mb v-wind (m s^{-1}). (right) The evolution of the surface soil wetness (dimensionless).

regions intensifying and prolonging the excessive heat into later summer. It remains to be seen whether GHGs may have set the stage for the development in these observed cases or whether naturally occurring drought would lead to the same outcome.

We investigate the predictability of this event by performing a supplemental set of 20 simulations, each initialized on 0000 UTC 15 May 2001 and run through August. Each simulation differs from the control (i.e., the ensemble member that produced the extreme event in Fig. 15) only in the initialization of the atmosphere; to produce the atmospheric initial conditions, a small perturbation was added to the control atmosphere's state on 15 May. The results are presented in Fig. 16. The left column shows the T_s anomalies from the control simulation, the center column shows those for the ensemble mean of the perturbation experiments, and the right column shows the ensemble mean of the soil moisture anomalies. In the ensemble mean, the wave structure in T_s is largely gone by June, indicating that in the span of a few weeks, the Rossby wave producing it has already lost all predictability. What remains in June is a general warm anomaly along the 40°–50°N latitudinal belt of continental Eurasia. This warming lasts into July and August over southern European Russia (the core of the original T_s anomaly) and is collocated with the dry soil wetness anomalies, suggesting that the land anomalies act to maintain the T_s anomalies several months beyond the predictability limit of the Rossby wave.

In summary, for at least some extreme heat wave and drought events, predictability associated with stationary Rossby waves, which are largely forced by submonthly transients, appears to be limited to perhaps 2–3 weeks. Nevertheless, there appears to be some longer-term predictability tied to the persistence of soil moisture anomalies. Ties to SST variations could provide some predictability on seasonal and longer time scales, although SST impacts appear to be intertwined with the underlying internally forced and shorter time scale Rossby wave structures, and this connection is currently poorly understood.

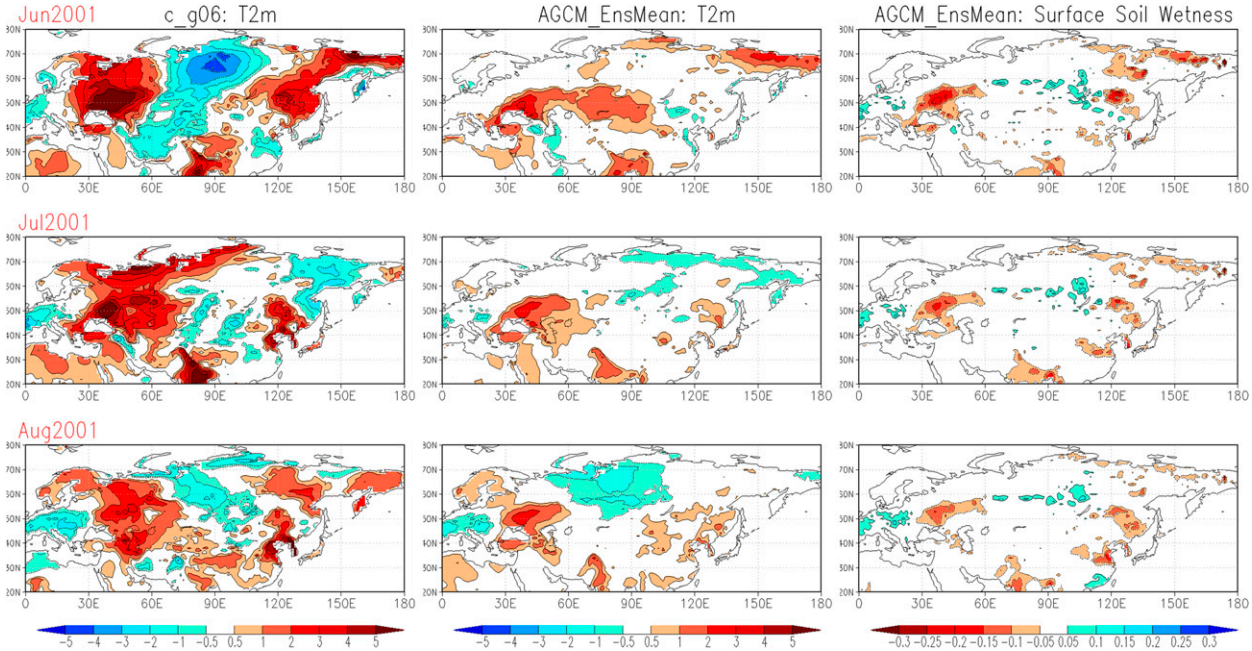

FIG. 16. Results from an ensemble of 20 perturbation experiments initialized on 0000 UTC 15 May 2001 for the ensemble member shown in Fig. 15. (left) The original evolution of the 2-m temperature (°C) from JJA 2001 (a repeat of part of Fig. 15). (center) As at (left), but for the ensemble mean of the perturbation runs. (right) As at (center), but for the ensemble mean surface soil wetness (dimensionless).

c. *A review of projections for the future*

We now address the question of how heat waves and droughts might manifest themselves in a future, warmer world.

Galos et al. (2007) reviewed drought occurrence in Hungary, noting that annual mean temperatures became warmer in the second half of the twentieth century, accompanied by a significant increase in drought frequency. In particular, summers for the period 1990–2004 were warmer than those of the previous 30 years. The period 1983–94 was an extraordinarily dry period, with severe droughts in the Carpathian basin of Hungary. They found from an analysis of the Max Planck Institute (MPI) regional model (REMO) twenty-first-century simulations [a limited area model forced by lateral boundary conditions from three different ECHAM5/MPI Ocean Model (MPI-OM) GCM runs—IPCC scenarios B1, A1B, and A2] that the probability of dry summers will not increase in the first half of the twenty-first century, but the intensity of dry events will increase due to the higher temperatures. They also found, however, that during the second half of the twenty-first century both the number and intensity of dry events will increase significantly.

Meehl and Tebaldi (2004) examined simulations of twentieth- and twenty-first-century climate produced by the global Parallel Climate Model (PCM), which used a "business as usual" emission scenario for the twenty-first century. They found the circulation patterns associated with heat waves in North America and Europe to be intensified in the twenty-first century, implying that future heat waves will be more intense, more frequent, and longer lasting in the second half of that century.

Barriopedro et al. (2011) show that the 2003 and 2010 summer heat waves likely produced the warmest seasonal temperatures seen in 500 years over about 50% of Europe. They conclude, based on regional climate model simulations driven by different GCMs forced by A1B emission scenarios, that the probability of a summer mega-heat wave over Europe will increase by a factor of 5 to 10 in the next 40 years, although the probability of an event with the magnitude seen in 2010 will remain relatively low until the second half of the twenty-first century.

The special report of the IPCC on extremes (Field et al. 2012) gives drought projections low confidence because of insufficient agreement among the individual projections resulting from both model differences and dependencies on the definition of drought (e.g., soil moisture versus precipitation-based indices). On the other hand, they conclude that is very likely that the length, frequency, and/or intensity of heat waves (defined with respect to present regional climate) will increase over most land areas. In particular over the high latitudes

of the Northern Hemisphere, a 1-in-20 year annual hottest day is likely to become a 1-in-5 year annual extreme by the end of the twenty-first century, under the Special Report on Emissions Scenarios (SRES) A2 and A1B emission scenarios.

6. Summary and concluding remarks

Drought and heat waves often go hand in hand. While this can of course simply be because drier soils produce less evaporative cooling of the surface, in northern Eurasia persistent anticyclones appear to play a key role, acting to both warm and dry the atmosphere and land surface over many important agricultural regions, from European Russia to Kazakhstan and beyond. The importance of anticyclones in the development of droughts was known as far back as the early twentieth century [e.g., Buchinsky 1976; see also the review of earlier literature in Obukhov et al. (1984)]. Different air masses are linked to the development of anticyclones, especially the intrusion of Arctic air masses that occasionally combine with subtropical air (e.g., associated with the Azores high in eastern Europe and western Russia); a basic understanding for how these air masses produce especially severe droughts across Eurasia was already established by that time [e.g., see the summary by Kleschenko et al. (2005)]. Perhaps less well understood, although mentioned in early historical documents, was the tendency for especially severe droughts and heat waves to be juxtaposed with wet and cool conditions in regions thousands of miles to the east or west (see section 1). Observational studies also established that while atmospheric droughts across northern Eurasia rarely last for more than 2 months (Cherenkova 2007), there is considerable evidence for longer (even multiyear) droughts to occur in the more southern marginal semiarid and arid regions of northern Eurasia [e.g., in Kazakhstan during the 1930s (cf. Kahan 1989; Almaty 2006) or over the Great Steppe of Central and East Asia (cf. Gumilev 1960)].

Here we provide an updated picture of the role of anticyclones in northern Eurasian summer climate through an analysis of the last three decades of monthly surface temperature and precipitation variability and covariability, using the latest generation of reanalyses and gridded station observations. We also examine longer-term changes (including the recent decadal changes) in surface temperature and precipitation over Eurasia and the interannual variability of these quantities over the last century or so, using model simulations (especially those with the GEOS-5 AGCM) to better understand the nature of the variability.

Among the key new results of this study is the quantification of the major summer patterns of monthly surface temperature and precipitation variability across northern Eurasia and the link between these patterns and stationary Rossby waves. The characteristic east–west wave structure of the leading patterns of surface meteorological variables are a reflection of these waves which, when amplified and stationary, appear to have led to some of the most extreme heat waves and droughts in Eurasia (e.g., the 2003 European and 2010 Russian heat waves), with anomalies of opposite sign occurring to the east and/or west depending on the phase and location of the wave. These waves appear to be initially forced upstream of Eurasia (e.g., within the North Atlantic jet exit region; Schubert et al. 2011); the wave energy propagates over northern Eurasia, north of the mean jet and/or farther to the south where it remains confined to the mean jet. The structure of these waves and their time scales (weeks to a few months) are consistent with past observations of the structure and time scales of heat waves and droughts across northern Eurasia.

The GEOS-5 AGCM simulations forced with observed SSTs and GHGs show heat waves that appear to be linked to Rossby waves occurring over Eurasia, including some rare, very extreme events during the last few decades. A case study of one of the most extreme heat waves to occur in the model (during the ''summer of 2001'' of one ensemble member) shows that the associated Rossby-like wave pattern in the surface temperature anomalies is for the most part unpredictable beyond about 1 month. Some aspects of the heat wave are, however, predictable for several months: these are the surface temperature anomalies at the center of the heat wave associated with soil moisture anomalies that persist through the summer. An inspection of the precursors to the heat wave show existing dry soil moisture anomalies (especially pronounced in that ensemble member) that are part of a long-term drying and warming trend simulated in the model, a trend that is consistent with observations. More generally, the impact of land–atmosphere feedbacks was quantified with model simulations in which the soil moisture feedbacks were disabled. These runs show that temperature variability is especially strongly tied to soil moisture variability in the southern parts of our study area extending from southern Europe eastward across the Caucasus, Kazakhstan, Mongolia, and northern China.

Our investigation of the warming that has been observed over northern Eurasia in the last three decades shows that it is part of a large-scale pattern of warming with local maxima over European Russia and over Mongolia/eastern Siberia. Precipitation changes consist of deficits across Eurasia covering parts of northeastern Europe, European Russia, Kazakhstan, southeastern Siberia, Mongolia, and northern China. Precipitation

increases occur across Siberia north of about 60°N. Remarkably, the ensemble mean of the AGCM simulations forced with observed SST and GHGs to a large extent reproduces the observed surface temperature and precipitation trend patterns of the last three decades, although with smaller amplitude. This suggests that some of the basic features of the observed trends over Eurasia are associated with an SST trend that consists of a PDO-like colder Pacific and an AMO-like warmer Atlantic. Various model simulations (Schubert et al. 2009) carried out with idealized versions of these basic SST patterns indicate a global-scale response to the PDO-like and AMO-like patterns, a response that is intensified by a global warming SST trend pattern. The dynamical response of the models to the SST forcing consists of a zonally symmetric positive upper tropospheric height anomaly in the midlatitudes of both hemispheres that appears to provide the large-scale atmospheric teleconnections linking the various regions of the world. We speculate that such a response was responsible for the synchronicity of droughts in such disparate regions as the Eurasian grain belt (spanning Russia, Ukraine, and Kazakhstan) and the U.S. Great Plains during, for example, the 1930s, as well as the drought and extreme heat in the same regions during the summer of 2012. It is also suggested that the longer time scales of dry conditions in the more southern regions of northern Eurasia may be induced by global SST anomalies.

A survey of the literature indicates a general consensus that the future holds an enhanced probability of heat waves across northern Eurasia especially by the second half of the twenty-first century, while there is less certainty regarding future drought, reflecting the greater uncertainty in precipitation and soil moisture projections compared with temperature. It is also clear that there are still gaps in our understanding of the physical mechanisms that control the intensity, duration, and frequency of heat waves and droughts. Perhaps most important are the uncertainties that remain in our understanding of the interactions between the short-term atmospheric variability associated with extremes and the longer-term variability and trends associated with soil moisture feedbacks, SST anomalies, and an overall warming world.

Acknowledgments. Support for this project was provided by the NASA Modeling, Analysis, and Prediction (MAP) Program. Research of Pavel Groisman was supported by NOAA/NASA (Grant NNX13AJ02G) and Grant 14.B25.31.0026 of the Ministry of Education and Science of the Russian Federation. The lead author would like to thank Anna Borovikov for helping to translate some of the Russian language literature. We also wish to thank two anonymous reviewers for their helpful comments and suggestions for improving the manuscript. The NOAA GHCN gridded V2 data, the NOAA Merged Air Land and SST Anomalies data, the NASA GPCP precipitation, and the NOAA PRECL precipitation data were obtained from NOAA/OAR/ESRL PSD from their website at http://www.esrl.noaa.gov/psd/. This paper is part of a special collection devoted to our understanding of drought throughout the world. The idea for this collection came about as a recommendation of a 2012 international workshop on the development of a Global Drought Information System (GDIS) sponsored by WCRP and various partner organizations (ESA-ESRIN, NASA, NIDIS, NSF, GEO, USCLIVAR, and NOAA).

APPENDIX A

Observational Datasets and Model Simulations

a. Observations and reanalyses

Our analysis is based in part on MERRA (Rienecker et al. 2011). MERRA is an atmospheric reanalysis that was produced with the Goddard Earth Observing System Data Assimilation System version 5 (GEOS-5) documented in Rienecker et al. (2008), consisting of the GEOS-5 atmospheric model and the Gridpoint Statistical Interpolation (GSI) analysis system, the latter being a system jointly developed by the GMAO and NOAA's National Centers for Environmental Prediction. The GEOS-5 assimilation system includes an incremental analysis update (IAU) procedure (Bloom et al. 1996) that slowly adjusts the model states toward the observed state. This has the benefit of minimizing any unrealistic spindown (or spinup) of the water cycle. MERRA was run at a resolution of ½° latitude × ⅔° longitude with 72 levels extending to 0.01 hPa. More information about MERRA can be found online (at http://gmao.gsfc.nasa.gov/research/merra/). The MERRA data used in this study (surface temperature, 2-m temperature, precipitation, and the 250-hPa meridional wind) were all taken at the full resolution of ½° latitude × ⅔° longitude covering the period 1979–2012. Limited comparisons are made with ERA-Interim (Dee et al. 2011a,b).

We also make use of various station observations. These are the NOAA–NCEP Climate Prediction Center (CPC) Global Historical Climatology Network (GHCN), version 2, and Climate Anomaly Monitoring System (GHCN_CAMS) gridded 2-m temperature (Fan and van den Dool 2008)—a 0.5° latitude × 0.5° longitude resolution dataset covering the period January 1948–January 2013. We also make use of the CRUTEM4 2-m temperature station data gridded to 5° latitude × 5° longitude

for the period 1850–2012 (Jones et al. 2012) and the NOAA Merged Land-Ocean Surface Temperature Analysis (MLOST; Smith et al. (2008)), version 3.5.2, also at 5° × 5° latitude/longitude for the period from 1880 to the present. For the precipitation data, we use NOAA's precipitation reconstruction over land (PRECL) on a 1° latitude–longitude grid for the period 1948–2013 (Chen et al. 2002). The other precipitation data used in the study are version 2.2 of the combined Global Precipitation Climatology Project (GPCP) data available on a 2.5° × 2.5° grid from 1979 to June 2011 (Adler et al. 2003).

b. *The GEOS-5 model and simulations*

We take advantage of an ensemble of 12 AMIP-style simulations carried out with the NASA Goddard Earth Observing System (GEOS-5) atmospheric general circulation model or AGCM (Rienecker et al. 2008; Molod et al. 2012) forced with observed SST for the period 1871–2012. The runs were started from different atmospheric and land initial conditions. Ten of the 12 ensemble members were run with interactive aerosols, while the other two used a prescribed aerosol climatology. We have found no discernable difference in the basic climatology and time dependence due to the treatment of the aerosols, so for the purposes of this study our ensemble means are based on all 12 runs. We also present some results on the impact of soil moisture feedback (section 3a). Those results are based on two 33-yr simulations for 1980–2012 forced with observed SST.[A1] The first was run with interactive land, while the second was run with specified climatological soil moisture computed as an average of a previously run multidecadal simulation. Details of the model are described next.

The GEOS-5 AGCM employs the finite-volume dynamics of Lin (2004). This dynamical core is integrated with various physics packages (Bacmeister et al. 2006) under the Earth System Modeling Framework (Collins et al. 2005) including the Catchment Land Surface Model (Koster et al. 2000) and a modified form of the relaxed Arakawa–Schubert convection scheme described by Moorthi and Suarez (1992). For the experiments described here we used version 2.4 of the AGCM. The model was run with 72 hybrid-sigma vertical levels extending to 0.01 hPa, and 1° (about 100 km) horizontal resolution on a latitude–longitude grid.

The CO_2 consists of the time-varying annual global mean values provided by IPCC CMIP5. The other greenhouse gases [GHGs: CH_4, N_2O, chlorofluorocarbon (CFC)-11, CFC-12, and hydrochlorofluorocarbon (HCFC)-22], stratospheric water vapor (H_2O), and ozone (O_3) are relaxed to time-varying zonal averages with a 3-day *e*-folding time. The zonal averages of the GHGs are taken from simulations of 1950–2010 with the GEOS chemistry–climate model (CCM; Pawson et al. 2008), and are calibrated (bias corrected) to the tropospheric concentrations specified by phase 5 of the Coupled Model Intercomparison Project (CMIP5; Meinshausen et al. 2011). Stratospheric H_2O is also taken from the CCM. In both cases, GHGs and H_2O, 5-yr running averages are first computed to reduce the influence of interannual variability in the CCM fields. Ozone is specified from Atmospheric Chemistry and Climate (AC&C)/Stratosphere–Troposphere Processes and their Role in Climate (SPARC) monthly averages (available online from ftp://ftp-esg.ucllnl.org/) from 1870 to 2005, and is converted to zonal means before interpolation onto GEOS-5 layers. For all seven gases, the relaxation fields have realistic latitudinal, vertical, and seasonal variations imposed on their specified trends. Two-day *e*-folding times allow the species contours to sufficiently follow planetary-scale potential vorticity deformations in the stratosphere.

Aerosols are computed using the Goddard Chemistry, Aerosol, Radiation, and Transport model (GOCART; Chin et al. 2002; Colarco et al. 2010) in GEOS-5. The GOCART module is run online within the GEOS-5 AGCM; that is, the aerosols and other tracers are radiatively interactive and transported consistently with the underlying hydrodynamics and physical parameterizations (e.g., moist convection and turbulent mixing) of the model. GOCART treats the sources, sinks, and chemistry of dust, sulfate, sea salt, and black and organic carbon aerosols. Aerosol species are assumed to be external mixtures. Total mass of sulfate and hydrophobic and hydrophilic modes of carbonaceous aerosols are tracked, while for dust and sea salt the particle size distribution is explicitly resolved across five noninteracting size bins for each.

Both dust and sea salt formulations have wind speed–dependent emission functions, while sulfate and carbonaceous species have emissions principally from fossil fuel combustion, biomass burning, and biofuel consumption, with additional biogenic sources of organic carbon. Sulfate has additional chemical production from oxidation of SO_2 and dimethyl sulfide (DMS), and we include a database of volcanic SO_2 emissions and injection heights. For all aerosol species, optical properties are primarily from the commonly used Optical Properties of Aerosols and Clouds (OPAC) dataset (Hess et al. 1998). This framework also includes the representation of CO tracers, which have emissions from fossil fuel, biofuel, and biomass burning. The online

[A1] In practice these two runs were reinitialized on 1 November of each year from a previous long model simulation forced with observed SST.

TABLE B1. Droughts and heat wave years in Eurasia (1875–2012). ENSO phase refers to summer months. Boldface indicates major droughts/heat waves as identified by various authors.

Year	Months	Regions affected	Source(s)	Comments
1875		Ukraine, non–black soil region, North Caucasus	Kahan 1989; Rudenko 1958	General Dmitry Milyutin's diary (see text); Strong La Niña
1879		Drought in Middle Volga, central Ukraine	Kahan 1989	La Niña
1885		South and East Ukraine, Middle and Lower Volga, North Caucasus	Kahan 1989	Tchaikovsky letter (http://therese-phil.livejournal.com/171196.html)*
1889		Drought in Ukraine, Lower Volga	Kahan 1989	La Niña
1890		Drought in central and southern regions of European Russia, Lower Volga, Ural; severe drought in Ukraine	Fedorov 1973; Buchinsky 1976; Kahan 1989; Boken et al. 2005	La Niña
1891	May–August	Drought in central and southern regions of European Russia, spreading north to middle course of Kama and Vyatka, black soil (chernozem) region, all of Volga, southern Ukraine, north Caucasus, 80% of European territory of USSR (ETU) within 45°–55°N, 30°–50°E affected by drought	Fedorov 1973; Buchinsky 1976; Meshcherskaya and Blazhevich 1997; Kahan 1989; Polozova and Grigoryeva 1984	Absolute temperature record for May was set (+31.8°C), not broken until 2007
1892		Drought in Central and southern regions of European Russia; Ukraine, central black soil region, Lower Volga, north Caucasus; 90% of ETU within 45°–55°N, 30°–50°E affected by drought (Polozova and Grigoryeva 1984)	Fedorov 1973; Buchinsky 1976; Kahan 1989; Polozova and Grigoryeva 1984	La Niña
1897		Drought in South Ukraine, Lower Volga; 80% of ETU within 45°–55°N, 30°–50°E affected by drought	Kahan 1989; Polozova and Grigoryeva 1984	
1898		Severe drought in Ukraine	Boken et al. 2005	
1900		Drought in Ukraine, western Siberia	Kahan 1989	El Niño
1901		"Southern" type of drought in the Volga River basin (Volga and Volga-Vyatka) and the Urals Region; eastern Ukraine, Ural, Lower and Middle Volga; 95% of ETU within 45°–55°N, 30°–50°E affected by drought	Golubev and Dronin, 2004; Kahan 1989; Polozova and Grigoryeva 1984	
1905		60% of ETU within 45°–55°N, 30°–50°E affected by drought	Polozova and Grigoryeva 1984	
1906		"Southern" type of drought in the Volga River basin (Volga and Volga-Vyatka) and the Urals Region; eastern Ukraine, Volga; 75% of ETU within 45°–55°N, 30°–50°E affected by drought	Golubev and Dronin 2004; Kahan 1989; Polozova and Grigoryeva 1984	Severe drought in Ukraine
1911		"Eastern" type of drought in steppe and forest-steppe of western and eastern Siberia; European Russia, Ukraine, west Siberia; severe drought in Ukraine; 65% of ETU within 45°–55°N, 30°–50°E affected by drought	Golubev and Dronin 2004; Kahan 1989; Boken et al. 2005; Polozova and Grigoryeva 1984	La Niña
1914		Volga, Ukraine; 75% of ETU within 45°–55°N, 30°–50°E affected by drought	Kahan 1989; Polozova and Grigoryeva 1984	El Niño

TABLE B1. (*Continued*)

Year	Months	Regions affected	Source(s)	Comments
1917		65% of ETU within 45°–55°N, 30°–50°E affected by drought	Polozova and Grigoryeva 1984	
1918		Ukraine	Rudenko 1958	
1920		Drought in central Russia, forest zone of European Russia; Ukraine, Volga; 95% of ETU between within 45°–55°N, 30°–50°E affected by drought	Golubev and Dronin, 2004; Kahan 1989; Polozova and Grigoryeva 1984	
1921		"Southern" type of drought in the Volga River basin (Volga and Volga-Vyatka) and the Urals region; European Russia, Ukraine, Volga, western Siberia; 95% of ETU within 45°–55°N, 30°–50°E affected by drought	Golubev and Dronin 2004; Kahan 1989; Rudenko 1958; Polozova and Grigoryeva 1984	1921 Famine in Russia (Volga-Ural region); La Niña; severe drought in Ukraine
1924		Drought in central Russia, forest zone of European Russia; Central Chernozem Region, Lower Volga; 90% of ETU within 45°–55°N, 30°–50°E affected by drought	Golubev and Dronin 2004; Kahan 1989; Polozova and Grigoryeva 1984	La Niña
1931	July	Heat wave; "Eastern" type of drought in steppe and forest-steppe of western and eastern Siberia; Ural, Central Chernozem Region; 75% of ETU between within 45°–55°N, 30°–50°E affected by drought	NOAA expert team (http://www.esrl.noaa.gov/psd/csi/events/2010/russianheatwave/prelim.html); Golubev and Dronin 2004; Kahan 1989; Meshcherskaya and Blazhevich 1997; Polozova and Grigoryeva 1984	
1933–39		Drought (low-water) years in western Kazakhstan	Almaty 2006	
1934		70% of ETU within 45°–55°N, 30°–50°E affected by drought	Polozova and Grigoryeva 1984	
1936		Drought in central Russia, forest zone of European Russia; Ukraine, Volga, western Siberia; 90% of ETU within 45°–55°N, 30°–50°E affected by drought	Golubev and Dronin 2004; Meshcherskaya and Blazhevich 1997; Kahan 1989; Polozova and Grigoryeva 1984	Dry preceding winter and spring; Cherenkova 2012
1938		Central Blacksoil Region, eastern Ukraine; 85% of ETU within 45°–55°N, 30°–50°E affected by drought	Kahan 1989; Polozova and Grigoryeva 1984	Dry preceding winter and spring; Cherenkova 2012; La Niña
1939		"Southern" type of drought in the Volga River basin (Volga and Volga-Vyatka) and the Urals Region; Lower Volga, Upper Volga, Southeast Ukraine; 65% of ETU within 45°–55°N, 30°–50°E affected by drought	Golubev and Dronin 2004; Kahan 1989; Polozova and Grigoryeva 1984	
1946		Drought in central Russia, forest zone of European Russia; Ukraine, Central Blacksoil Region, Volga, North Caucasus; 100% of ETU within 45°–55°N, 30°–50°E affected by drought	Golubev and Dronin 2004; Kahan 1989; Polozova and Grigoryeva 1984	Famine; serious crop failures in grain production in USSR; drought covered 50% of total agricultural land of USSR
1948		"Southern" type of drought in the Volga River basin (Volga and Volga-Vyatka) and the Urals Region	Golubev and Dronin 2004; Kahan 1989	Serious crop failures in grain production in USSR
1950		Eastern Ukraine, Middle and Lower Volga; 85% of ETU within 45°–55°N, 30°–50°E affected by drought	Kahan 1989; Polozova and Grigoryeva 1984	La Niña

TABLE B1. (*Continued*)

Year	Months	Regions affected	Source(s)	Comments
1951		"Southern" type of drought in the Volga River basin (Volga and Volga-Vyatka) and the Urals Region; drought in Asian part of FSU; Ukraine, Lower Volga; 75% of ETU within 45°–55°N, 30°–50°E affected by drought	Golubev and Dronin 2004; Meshcherskaya and Blazhevich 1997; Kahan 1989; Polozova and Grigoryeva 1984	El Niño
1953		Ukraine, Volga	Kahan 1989	
1954		Southern Ukraine, Lower Volga; 60% of ETU within 45°–55°N, 30°–50°E affected by drought	Kahan 1989; Polozova and Grigoryeva 1984	La Niña
1955	July	Heat wave over Russia; drought in Asian part of FSU; western Siberia, Lower Volga	Meshcherskaya and Blazhevich 1997; Kahan 1989	La Niña
1957		"Southern" type of drought in the Volga River basin (Volga and Volga-Vyatka) and the Urals Region; 75% of ETU within 45°–55°N, 30°–50°E affected by drought	Golubev and Dronin 2004; Polozova and Grigoryeva 1984	Serious crop failures in grain production in USSR; El Niño
1959		60% of ETU within 45°–55°N, 30°–50°E affected by drought	Polozova and Grigoryeva 1984	Serious crop failures in grain production in USSR
1960		Heat wave in western Russia	NOAA expert team	Associated with blocking
1963		"Eastern" type of drought in steppe and forest-steppe of western and eastern Siberia; western Siberia, Kazakhstan, Ural, eastern Ukraine; 95% of ETU within 45°–55°N, 30°–50°E affected by drought	Golubev and Dronin 2004; Kahan 1989; Polozova and Grigoryeva 1984	Serious crop failures in grain production in USSR; El Niño
1965		"Eastern" type of drought in steppe and forest-steppe of western and eastern Siberia; drought in Asian part of FSU; western Siberia, Kazakhstan, central Asia, Ural, Volga	Golubev and Dronin 2004; Meshcherskaya and Blazhevich 1997; Kahan 1989	El Niño
1972–78		Drought (low-water) years in western and northern Kazakhstan	Almaty 2006	
1972	Established in May and lasted through summer	Drought and heat wave: Anticyclone centered over Moscow, covered western Russia, drought started in eastern Ukraine; 100% of ETU within 45°–55°N, 30°–50°E affected by drought	Fedorov 1973; Buchinsky 1976; Strashnaya and Bogomolova 2005; Polozova and Grigoryeva 1984; Cherenkova 2012	Blocking, *one of worst modern droughts*—"100-year" drought; El Niño; serious crop failures in grain production in USSR; Dry preceding winter and spring.
1975		"Southern" type of drought in the Volga River basin (Volga and Volga-Vyatka) and the Urals Region	Golubev and Dronin 2004; Meshcherskaya and Blazhevich 1997; Strashnaya and Bogomolova 2005	Serious crop failures in grain production in USSR; La Niña
1979		Drought in central Russia, forest zone of European Russia	Golubev and Dronin 2004; Meshcherskaya and Blazhevich 1997; Strashnaya and Bogomolova 2005	Serious crop failures in grain production in USSR
1981	July heat wave	Drought and heat wave in central Russia, forest zone of European Russia	Golubev and Dronin 2004; Meshcherskaya and Blazhevich 1997; Strashnaya and Bogomolova 2005; NOAA expert team	No unusual blocking; Worst drought in European Russia between 1891 and 1995; serious crop failures in grain production in USSR
1984		Drought in Central Russia, forest zone of European Russia, northern and western United Kingdom	Golubev and Dronin 2004; Ben Lloyd-Hughes, Benfield Hazard Research Centre, UCL	United Kingdom: Very dry spring and summer led to the imposition of hosepipe bans.

TABLE B1. (*Continued*)

Year	Months	Regions affected	Source(s)	Comments
1988	July	Russia	NOAA expert team	Blocking, La Niña
1991		"Eastern" type of drought in steppe and forest-steppe of western and eastern Siberia	Golubev and Dronin 2004;	El Niño
1992		Germany, Hungary, Bulgaria, and much of western Russia	Ben Lloyd-Hughes, Benfield Hazard Research Centre, UCL	German crop production reduced by 22%. Irrigation suspended in Bulgaria. Worst Russian drought in 10 years
1995		"Southern" type of drought in the Volga basin (Volga and Volga-Vyatka) and the Urals Region	Golubev and Dronin 2004; Strashnaya and Bogomolova 2005	El Niño
1996–97		Drought (low-water) years in western and northern Kazakhstan	Almaty 2006	
1998		The Volga region, north Caucasus, and central Chernozem, warmest year of the last century for Mongolia	Strashnaya and Bogomolova 2005, Batima et al. 2005	
1999–2002		Summer drought in Mongolia	Batima et al. 2005	1999, 2000 La Niña; 2002 El Niño
1999	July	Heat wave in western Russia	NOAA expert team	No unusual blocking over Russia; La Niña
2001		July heat wave in western Russia, drought in southern Kazakhstan	NOAA expert team; Almaty 2006	No unusual blocking over Russia
2002	July	July heat wave in western Russia, drought in southern Kazakhstan	NOAA expert team; Almaty 2006	No unusual blocking over Russia
2007	May, June, continued to September in Japan	Heat wave in southeast Europe (June–August), South Asian countries of India, Pakistan, Bangladesh and Nepal, as well as Russia, Japan, and China	Buranov, I., A. Geroyeva, and A. Kornysheva (29 May 2007): "Moscow Swelters in Heat Wave," Kommersant.com.	The temperature in Moscow reached +32.9°C (91.2°F) on 27 May. The Russian capital had not seen such a sustained heat wave for 128 years. On 28 May an absolute temperature record for May was set, breaking the record of +31.8°C (89.2°F) that had been registered back in 1891
2010	July	Eastern Europe, Russia heat wave	Barriopedro et al. 2011; Meshcherskaya et al. 2011; Mokhov 2011	Pakistan: all-time high of 53.7°C at Mohenjo-Daro, Sindh, 26 May; Cold preceding winter in European territory of Russia; Cherenkova 2012
2012	Summer	Drought and heat wave over Russia, Kazakhstan, Ukraine	http://theextinctionprotocol.wordpress.com/2012/07/31/severe-heatwave-drought-and-wildfires-destroy-russian-harvest/	Eurasian grain belt hit hard

* In a letter from Tchaikovsky (composer) to N. von Mekk, 3–10 August 1885, in Majdanovo, now Klin: "I'm writing to you at three o'clock in the afternoon in such darkness, you would think it was nine o'clock at night. For several days, the horizon has been enveloped in a smoke haze, arising, they say, from fires in the forest and peat bogs. Visibility is diminishing by the day, and I'm starting to fear that we might even die of suffocation" (http://therese-phil.livejournal.com/171196.html).

CO processes in GEOS-5 derive from Bian et al. (2007), and include indirect production of CO from oxidation of natural and anthropogenic nonmethane hydrocarbons, chemical production from methane (CH_4) oxidation, and losses through reaction with OH.

APPENDIX B

Northern Eurasian Droughts and Heat Waves since 1875

Here we briefly review some of the key metrics that have been used to characterize drought and heat waves over northern Eurasia. We also include some further information (in addition to that already provided in the text) on past droughts and heat waves over this region. Table B1 is a compilation of the droughts and heat waves that have occurred since 1875, based on various scientific publications as well as the popular literature (references are noted in the table). The table also includes information on the regions affected, and other auxiliary information (comments) of potential use to those interested in investigating these events further. Years in bold indicate major droughts or heat waves, although it must be kept in mind that these are very subjective assessments of the relative severity of the various events, since they are based on differing metrics that emphasize varying aspects of meteorological, agricultural, and hydrological droughts (and heat waves), over different time periods. As such, Table B1 should be considered as a convenient starting point for further investigation of the various droughts and heat waves that have occurred over northern Eurasia in the last 135 years or so, rather than an objective comparative assessment of all droughts and heat waves that have occurred over this very large region. In fact, we view this table (in the spirit of the GDIS effort mention earlier) as the starting point for a continually evolving catalog of historical droughts and heat waves that have occurred worldwide.

Turning now to some of the popular metrics of drought, Ped (1975) introduced the index of aridity S_i defined as

$$S_i = \frac{\Delta T}{\sigma_T} - \frac{\Delta P}{\sigma_P}, \tag{B1}$$

where ΔT and ΔP are the deviations (from a long-term mean) of monthly mean air temperatures and precipitation, and σ_T and σ_P are their standard deviations. This index has been used frequently in the CIS for identification of atmospheric drought in terms of three classes: light ($0 \le S_i < 2.0$), average ($2.0 \le S_i < 3.0$), and strong ($S_i \ge 3.0$).

Another popular index is the hydrothermal coefficient (HTC) developed by Selianinov (1928):

$$\mathrm{HTC} = \sum R / 0.1 \sum T, \tag{B2}$$

where the numerator is the total rainfall over the growing season (in mm) and the sum in the denominator is the accumulated mean daily surface air temperature above 10°C for the same time period. The threshold for drought is typically HTC values less than or equal to 0.8, with severe droughts having HTC values of 0.4 or less.

Meshcherskaya and Blazhevich (1997) developed a combined drought and excessive moisture index (DM) that takes into account the areal extent of the precipitation and temperature anomalies. Drought (excessive wet) conditions are defined according to whether the precipitation falls below (exceeds) 80% (120%) of the long-term mean, and the temperature anomalies are above (below) 1°C (−1°C). They produced a catalog of drought occurrence over the main grain-producing regions of the FSU for May–July 1891–1995 for both the European and Asian parts (see their Table 4). They found that the most severe droughts (in order of decreasing severity) in the European region occurred during 1936, 1975, 1979, and 1891, while for the Asian part the most severe droughts occurred during 1955, 1965, 1951, and 1931.

Dai (2011) compared different forms of the Palmer drought severity index (PDSI), finding generally little difference between four different formulations. They generally compare well with monthly soil moisture observations (Robock et al. 2000), annual streamflow, and monthly *Gravity Recovery and Climate Experiment* (*GRACE*) satellite-observed water storage changes. For example, correlations of up to 0.77 were found in parts of the FSU for soil moisture in the top 1 m even over high-latitude cold regions (east of the Urals).

Another more recently developed drought index that includes the effects of temperature on drought variability is the standardized precipitation evapotranspiration index (SPEI; Vicente-Serrano et al. 2010). The SPEI, similar to the self-calibrating (sc-)PDSI (Wells et al. 2004), can capture increases in drought severity associated with higher water demand as a result of evapotranspiration, under global warming conditions. The SPEI was used, for example, by Potop and Možný (2011) to study the evolution of drought in the Czech Republic. They found that increasing temperatures played a role in the intensification of the droughts during the 1980s and 1990s.

Rocheva (2012) proposed a 500-mb height index as an indicator of drought over the main grain-producing

regions of Russia using NCEP–NCAR reanalysis data. They found that droughts occurred during 1972, 1975, 1979, 1981, 1995, and 1998 [they note that their findings are consistent with the droughts identified by Strashnaya and Bogomolova (2005)].

According to Golubev and Dronin (2004), droughts in Russia during the last hundred years tended to occur over three main geographical areas consisting of central, southern, and eastern Russia (based on TsUEG 1933). The central type of drought covers the Volga basin, the northern Caucasus, and the Central Chernozem Region and some oblasts of the central region, affecting the major agricultural regions of Russia, and the forest zone of European Russia (associated with numerous forest fires in the central and northern regions). The southern type of drought is limited to the Volga basin and Urals region and, while it covers less area, its intensity has generally been more severe and has often destroyed the entire crop production of the affected region. They note that the eastern type of drought affects the steppe and forest-steppe of Siberia and this usually occurs when the southern part of European Russia is characterized by good weather. This again highlights the juxtaposition of drought and wet conditions as a characteristic feature of climate variability over Eurasia; in this case the contrast is between European and Asian Russia. Golubev and Dronin (2004) summarize the past occurrence of each type of drought with the central droughts occurring during 1920, 1924, 1936, 1946, 1972, 1979, 1981, and 1984, the southern droughts occurring during 1901, 1906, 1921, 1939, 1948, 1951, 1957, 1975, and 1995, and the eastern droughts occurring during 1911, 1931, 1963, 1965, and 1991. One of the worst modern droughts over ER occurred in the summer of 1972 (Fedorov 1973; Buchinsky 1976). That drought was associated with an anticyclone that was centered over Moscow and that established in May and persisted throughout the summer. The drought appears to have started in eastern Ukraine and was at the time characterized as a 100-yr event.

A NOAA team of experts (http://www.esrl.noaa.gov/psd/csi/events/2010/russianheatwave/prelim.html) note that western Russia has a climatological vulnerability to blocking (see also Tyrlis and Hoskins 2008; Woollings et al. 2008; Dole et al. 2011) and associated heat waves (e.g., 1960, 1972, and 1988). They point out, however, that a high index value for blocking days is not a necessary condition for high July surface temperature over western Russia—for example, the warm summers of 1981, 1999, 2001, and 2002 did not experience an unusual number of blocking days.

Almaty (2006) found that hydrological drought (low runoff) occurred in the western regions of Kazakhstan during 1933–39, 1972–78, and 1996–97. The latter two periods were also low-water periods in northern Kazakhstan, whereas 1963–65, 1967–70, and 1996–2000 were low-water periods in central Kazakhstan. Drought comes to the lowland of southern Kazakhstan roughly every 4–5 years. It was in drought during 2000–01 with the Chardarya reservoir having the lowest water storage since 1977 in August of 2001.

REFERENCES

Adler, R. F., and Coauthors, 2003: The version 2 Global Precipitation Climatology Project (GPCP) Monthly Precipitation Analysis (1979–present). *J. Hydrometeor.,* **4,** 1147–1167, doi:10.1175/1525-7541(2003)004<1147:TVGPCP>2.0.CO;2.

Alexander, L. V., and Coauthors, 2006: Global observed changes in daily climate extremes of temperature and precipitation. *J. Geophys. Res.,* **111,** D05109, doi:10.1029/2005JD006290.

Almaty, 2006: Drought management and mitigation assessment for Kazakhstan, phase two: Regional vulnerability and capacity assessment survey. Nature Protection Ministry Republic of Kazakhstan, Kazgidromet, 196 pp. [Available online at http://siteresources.worldbank.org/EXTECAREGTOPRURDEV/Resources/573581-1164120557290/KazakstanDroughtPlan-English.pdf.]

Ambrizzi, T., B. J. Hoskins, and H.-H. Hsu, 1995: Rossby wave propagation and teleconnection patterns in the austral winter. *J. Atmos. Sci.,* **52,** 3661–3672, doi:10.1175/1520-0469(1995)052<3661:RWPATP>2.0.CO;2.

Bacmeister, J. T., M. J. Suarez, and F. R. Robertson, 2006: Rain reevaporation, boundary layer–convection interactions, and Pacific rainfall patterns in an AGCM. *J. Atmos. Sci.,* **63,** 3383–3403, doi:10.1175/JAS3791.1.

Barash, S. I., 1989: *History of Bad Harvests and Weather in Europe* (in Russian). Gidrometeoizdat, 236 pp.

Barriopedro, D., E. M. Fischer, J. Luterbacher, R. M. Trigo, and R. Garcia-Herrera, 2011: The hot summer of 2010: Redrawing the temperature record map of Europe. *Science,* **332,** 220–224, doi:10.1126/science.1201224.

Batima, P., L. Natsagdorj, P. Gombluudev, and B. Erdenetsetseg, 2005: Observed climate change in Mongolia. Assessments of Impacts and Adaptations to Climate Change (AIACC) Working Paper, 26 pp. [Available online at http://www.aiaccproject.org/working_papers/Working%20Papers/AIACC_WP_No013.pdf.]

Bian, H., M. Chin, R. Kawa, B. Duncan, A. Arellano Jr., and R. Kasibhatla, 2007: Uncertainty of global CO simulations constraint by biomass burning emissions. *J. Geophys. Res.,* **112,** D23308, doi:10.1029/2006JD008376.

Bloom, S., L. Takacs, A. DaSilva, and D. Ledvina, 1996: Data assimilation using incremental analysis updates. *Mon. Wea. Rev.,* **124,** 1256–1271, doi:10.1175/1520-0493(1996)124<1256:DAUIAU>2.0.CO;2.

Bogolepov, V. A., 1922: Causes of poor harvest and starvation in Russia in the historical period (in Russian). Novaya Derevnya, 38 pp.

Boken, V., A. P. Cracknell, and R. L. Heathcote, Eds., 2005: *Monitoring and Predicting Agricultural Drought: A Global Study.* Oxford University Press, 472 pp.

Borisenkov, E. P., and V. M. Pasetsky, 1988: *Thousand-Year Chronicle of Unusual Phenomena of Nature* (in Russian). Gidrometeoizdat, 522 pp.

Bothe, O., K. Fraedrich, and X. Zhu, 2010: The large-scale circulations and summer drought and wetness on the Tibetan plateau. *Int. J. Climatol.,* **30,** 844–855.

Briffa, K. R., P. D. Jones, F. H. Schweingruber, S. G. Shiyyatov, and E. R. Cook, 1995: Unusual twentieth-century summer warmth in a 1,000-year temperature record from Siberia. *Nature,* **376,** 156–159, doi:10.1038/376156a0.

Buchinsky, I. E., 1976: *Droughts and Dry Winds* (in Russian). Gidrometeoizdat, 214 pp.

Chen, M., P. Xie, J. E. Janowiak, and P. A. Arkin, 2002: Global land precipitation: A 50-yr monthly analysis based on gauge observations. *J. Hydrometeor.,* **3,** 249–266, doi:10.1175/1525-7541(2002)003<0249:GLPAYM>2.0.CO;2.

Cherenkova, E. A., 2007: Dynamics of severe atmospheric droughts in European Russia. *Russ. Meteor. Hydrol.,* **32** (11), 675–682.

——, 2012: Analysis of extensive atmospheric droughts features in the south of European Russia. *Arid Ecosyst.,* **2** (4), 209–215.

Chin, M., and Coauthors, 2002: Tropospheric aerosol optical thickness from the GOCART model and comparisons with satellite and sun photometer measurements. *J. Atmos. Sci.,* **59,** 461–483, doi:10.1175/1520-0469(2002)059<0461:TAOTFT>2.0.CO;2.

Colarco, P., A. da Silva, M. Chin, and T. Diehl, 2010: Online simulations of global aerosol distributions in the NASA GEOS-4 model and comparisons to satellite and ground-based aerosol optical depth. *J. Geophys. Res.,* **115,** D14207, doi:10.1029/2009JD012820.

Collins, N., and Coauthors, 2005: Design and implementation of components in the Earth System Modeling Framework. *Int. J. High Perform. Comput. Appl.,* **19,** 341–350, doi:10.1177/1094342005056120.

Dai, A., 2011: Characteristics and trends in various forms of the Palmer Drought Severity Index during 1900–2008. *J. Geophys. Res.,* **116,** D12115, doi:10.1029/2010JD015541.

de Beurs, K. M., and G. M. Henebry, 2008: Northern annular mode effects on the land surface phenologies of northern Eurasia. *J. Climate,* **21,** 4257–4279, doi:10.1175/2008JCLI2074.1.

Dee, D. P., and Coauthors, 2011a: The ERA-Interim reanalysis: Configuration and performance of the data assimilation system. *Quart. J. Roy. Meteor. Soc.,* **137,** 553–597, doi:10.1002/qj.828.

——, P. Poli, and A. J. Simmons, 2011b: Extension of the ERA-Interim reanalysis to 1979. *ECMWF Newsletter,* No. 128, ECMWF, Reading, United Kingdom, 7. [Available online at http://www.ecmwf.int/publications/newsletters/pdf/128.pdf.]

Demezhko, D. Yu., and I. V. Golovanova, 2007: Climatic changes in the Urals over the past millennium – an analysis of geothermal and meteorological data. *Climate Past,* **3,** 237–242, doi:10.5194/cp-3-237-2007.

Deser, C., R. A. Tomas, and S. Peng, 2007: The transient atmospheric circulation response to North Atlantic SST and sea ice anomalies. *J. Climate,* **20,** 4751–4767, doi:10.1175/JCLI4278.1.

Ding, Q., and B. Wang, 2005: Circumglobal teleconnection in the Northern Hemisphere summer. *J. Climate,* **18,** 3483–3505, doi:10.1175/JCLI3473.1.

——, and ——, 2007: Intraseasonal teleconnection between the summer Eurasian wave train and the Indian monsoon. *J. Climate,* **20,** 3751–3767, doi:10.1175/JCLI4221.1.

Dole, R., and Coauthors, 2011: Was there a basis for anticipating the 2010 Russian heat wave? *Geophys. Res. Lett.,* **38,** L06702, doi:10.1029/2010GL046582.

Fan, Y., and H. van den Dool, 2008: A global monthly land surface air temperature analysis for 1948–present. *J. Geophys. Res.,* **113,** D01103, doi:10.1029/2007JD008470.

Farat, R., M. Kepinska-Kasprzak, P. Kowalczak, and P. Mager, 1998: Droughts in Poland, 1951–90. *Drought Network News,* Vol. 10, National Drought Mitigation Center, Linclon, NE, Paper 42, 5 pp. [Available online at http://digitalcommons.unl.edu/droughtnetnews/42.]

Fedorov, E. K., 1973: *Weather and Yield* (in Russian). Gidrometeoizdat, 55 pp.

Ferranti, L., and P. Viterbo, 2006: The European summer of 2003: Sensitivity to soil water initial conditions. *J. Climate,* **19,** 3659–3680, doi:10.1175/JCLI3810.1.

Field, C. B., and Coauthors, Eds., 2012: *Managing the Risks of Extreme Events and Disasters to Advance Climate Change Adaptation.* Cambridge University Press, 582 pp.

Fischer, E. M., S. I. Seneviratne, P. L. Vidale, D. Lüthi, and C. Schär, 2007: Soil moisture–atmosphere interactions during the 2003 European summer heat wave. *J. Climate,* **20,** 5081–5099, doi:10.1175/JCLI4288.1.

Folland, C. K., and Coauthors, 2001: Observed climate variability and change. *Climate Change 2001: The Scientific Basis,* J. T. Houghton et al., Eds., Cambridge University Press, 99–181.

Francis, J. A., and S. J. Vavrus, 2012: Evidence linking Arctic amplification to extreme weather in mid-latitudes. *Geophys. Res. Lett.,* **39,** L06801, doi:10.1029/2012GL051000.

Frey, K. E., and L. C. Smith, 2003: Recent temperature and precipitation increases in west Siberia and their association with the Arctic Oscillation. *Polar Res.,* **22,** 287–300, doi:10.1111/j.1751-8369.2003.tb00113.x.

Frich, P., L. V. Alexander, P. Della-Marta, B. Gleason, M. Haylock, A. M. G. Klein Tank, and T. Peterson, 2002: Observed coherent changes in climatic extremes during the second half of the twentieth century. *Climate Res.,* **19,** 193–212, doi:10.3354/cr019193.

Galarneau, T. J., T. M. Hamill, R. M. Dole, and J. Perlwitz, 2012: A multiscale analysis of the extreme weather events over western Russia and northern Pakistan during July 2010. *Mon. Wea. Rev.,* **140,** 1639–1664, doi:10.1175/MWR-D-11-00191.1.

Galos, B., P. Lorenz, and D. Jacob, 2007: Will dry events occur more often in Hungary in the future? *Environ. Res. Lett.,* **2,** 034006, doi:10.1088/1748-9326/2/3/034006.

Gershunov, A., and H. Douville, 2008: Extensive summer hot and cold extremes under current and possible future climatic conditions: Europe and North America. *Climate Extremes and Society,* H. F. Diaz and R. J. Murnane, Eds., Cambridge University Press, 74–98.

Ghelli, A., A. Garcia-Mendez, F. Prates, and M. Dahoui, 2011: Extreme weather events in summer 2010: How did the ECMWF forecasting systems perform? *ECMWF Newsletter,* No. 125, ECMWF, Reading, United Kingdom, 7–11. [Available online at http://www.ecmwf.int/publications/newsletters/pdf/125.pdf.]

Golubev, G., and N. Dronin, 2004: Geography of droughts and food problems in Russia (1900–2000). Department of Geography, Moscow State University, Moscow, Russia (published by the Center for Environmental Systems Research, Kassel, Germany), 29 pp.

Groisman, P. Ya., and Coauthors, 1999: Changes in the probability of heavy precipitation: Important indicators of climatic change. *Climatic Change,* **42,** 243–283, doi:10.1023/A:1005432803188.

——, and Coauthors, 2007: Potential forest fire danger over northern Eurasia: Changes during the 20th century. *Global Planet. Change,* **56,** 371–386, doi:10.1016/j.gloplacha.2006.07.029.

——, and Coauthors, 2009: The Northern Eurasian Earth Science Partnership: An example of science applied to societal

needs. *Bull. Amer. Meteor. Soc.,* **90,** 671–688, doi:10.1175/2008BAMS2556.1.

——, R. W. Knight, and O. G. Zolina, 2013: Recent trends in regional and global extreme precipitation patterns. *Climate Vulnerability: Understanding and Addressing Threats to Essential Resources,* R. Pielke Sr. et al., Eds., Elsevier, 25–55.

Gumilev, L. N., 1960: *The Huns: Central Asia in Ancient Times* (in Russian). Izdatel'stvo Vostochnoi Literatury, 290 pp.

Hess, M., P. Koepke, and I. Schult, 1998: Optical properties of aerosols and clouds: The software package OPAC. *Bull. Amer. Meteor. Soc.,* **79,** 831–844, doi:10.1175/1520-0477(1998)079<0831:OPOAAC>2.0.CO;2.

Hirschi, M., and Coauthors, 2011: Observational evidence for soil-moisture impact on hot extremes in southeastern Europe. *Nat. Geosci.,* **4,** 17–21, doi:10.1038/ngeo1032.

Ionita, M., G. Lohmann, N. Rimbu, S. Chelcea, and M. Dima, 2012: Interannual to decadal summer drought variability over Europe and its relationship to global sea surface temperature. *Climate Dyn.,* **38,** 363–377, doi:10.1007/s00382-011-1028-y.

Johansson, Å., 2007: Prediction skill of the NAO and PNA from daily to seasonal time scales. *J. Climate,* **20,** 1957–1975, doi:10.1175/JCLI4072.1.

Jones, P. D., D. H. Lister, T. J. Osborn, C. Harpham, M. Salmon, and C. P. Morice, 2012: Hemispheric and large-scale land surface air temperature variations: An extensive revision and an update to 2010. *J. Geophys. Res.,* **117,** D05127, doi:10.1029/2011JD017139.

Kahan, A., 1989: *Russian Economic History: The Nineteenth Century.* R. Weiss, Ed., University of Chicago Press, 251 pp.

Kleschenko, A. D., and Coauthors, 2005: Monitoring agricultural drought in Russia. *Monitoring and Predicting Agricultural Drought,* V. Boken, A. P. Cracknell, and R. L. Heathcote, Eds., Oxford University Press, 196–207.

Körnich, H., 2010: Predictability of the coupled troposphere–stratosphere system. *Proc. ECMWF Seminar on Predictability in the European and Atlantic Regions,* Reading, United Kingdom, ECMWF, 127–136. [Available online at http://www.ecmwf.int/publications/library/ecpublications/_pdf/seminar/2010/Koernich.pdf.]

Koster, R. D., M. J. Suárez, A. Ducharne, M. Stieglitz, and P. Kumar, 2000: A catchment-based approach to modeling land surface processes in a GCM: 1. Model structure. *J. Geophys. Res.,* **105,** 24 809–24 822, doi:10.1029/2000JD900327.

——, and Coauthors, 2004: Regions of strong coupling between soil moisture and precipitation. *Science,* **305,** 1138–1140, doi:10.1126/science.1100217.

——, B. M. Fekete, G. J. Huffman, and P. W. Stackhouse Jr., 2006a: Revisiting a hydrological analysis framework with International Satellite Land Surface Climatology Project Initiative 2 rainfall, net radiation, and runoff fields. *J. Geophys. Res.,* **111,** D22S05, doi:10.1029/2006JD007182.

——, M. J. Suarez, and S. D. Schubert, 2006b: Distinct hydrological signatures in observed historical temperature fields. *J. Hydrometeor.,* **7,** 1061–1075, doi:10.1175/JHM530.1.

——, and Coauthors, 2011: The second phase of the Global Land-Atmosphere Coupling Experiment: Soil moisture contributions to subseasonal forecast skill. *J. Hydrometeor.,* **12,** 805–822, doi:10.1175/2011JHM1365.1.

Lau, W. K. M., and K.-M. Kim, 2012: The 2010 Pakistan flood and Russian heat wave: Teleconnection of hydrometeorological extremes. *J. Hydrometeor.,* **13,** 392–403, doi:10.1175/JHM-D-11-016.1.

Lin, S.-J., 2004: A ''vertically Lagrangian'' finite-volume dynamical core for global models. *Mon. Wea. Rev.,* **132,** 2293–2307, doi:10.1175/1520-0493(2004)132<2293:AVLFDC>2.0.CO;2.

Liu, A. Z., M. Ting, and H. Wang, 1998: Maintenance of circulation anomalies during the 1988 drought and 1993 floods over the United States. *J. Atmos. Sci.,* **55,** 2810–2832, doi:10.1175/1520-0469(1998)055<2810:MOCADT>2.0.CO;2.

Lorenz, R., E. B. Jaeger, and S. I. Seneviratne, 2010: Persistence of heat waves and its link to soil moisture memory. *Geophys. Res. Lett.,* **37,** L09703, doi:10.1029/2010GL042764.

Lupo, A. R., I. Mokhov, M. G. Akperov, A. V. Chernokulsky, and H. Athar, 2012: A dynamic analysis of the role of the planetary- and synoptic-scale in the summer of 2010 blocking episodes over the European part of Russia. *Adv. Meteor.,* **2012,** 584257, doi:10.1155/2012/584257.

Lydolph, P. E., 1964: Russian Sukhovey. *Ann. Assoc. Amer. Geogr.,* **54,** 291–309, doi:10.1111/j.1467-8306.1964.tb00490.x.

Lyon, B. F., and R. M. Dole, 1995: A diagnostic comparison of the 1980 and 1988 U.S. Summer heat wave–droughts. *J. Climate,* **8,** 1658–1676, doi:10.1175/1520-0442(1995)008<1658:ADCOTA>2.0.CO;2.

Matsueda, M., 2011: Predictability of Euro-Russian blocking in summer of 2010. *Geophys. Res. Lett.,* **38,** L06801, doi:10.1029/2010GL046557.

Meehl, G., and C. Tebaldi, 2004: More intense, more frequent, and longer lasting heat waves in the 21st century. *Science,* **305,** 994–997, doi:10.1126/science.1098704.

Meinshausen, M., and Coauthors, 2011: The RCP greenhouse gas concentrations and their extension from 1765 to 2300. *Climatic Change,* **109,** 213–241, doi:10.1007/s10584-011-0156-z.

Meshcherskaya, A. V., and V. G. Blazhevich, 1997: The drought and excessive moisture indices in a historical perspective in the principal grain-producing regions of the former Soviet Union. *J. Climate,* **10,** 2670–2682, doi:10.1175/1520-0442(1997)010<2670:TDAEMI>2.0.CO;2.

——, M. P. Golod, and V. M. Mirvis, 2011: The drought in 2010 against the background of multiannual changes in aridity in the major grain producing regions of the European part of Russia (in Russian). *Proc. Main Geophys. Obs.,* **563,** 1–27.

Mokhov, I. I., 2011: Specific features of the 2010 summer heat formation in the European territory of Russia in the context of general climate changes and climate anomalies. *Izv. Atmos. Ocean. Phys.,* **47,** 653–660, doi:10.1134/S0001433811060119.

Molod, A., L. Takacs, M. Suarez, J. Bacmeister, I.-S. Song, and A. Eichmann, 2012: The GEOS-5 atmospheric general circulation model: Mean climate and development from MERRA to Fortuna. NASA Tech. Rep. Series on Global Modeling and Data Assimilation, Vol. 28, NASA TM–2012-104606, 117 pp.

Moorthi, S., and M. J. Suarez, 1992: Relaxed Arakawa-Schubert: A parameterization of moist convection for general circulation models. *Mon. Wea. Rev.,* **120,** 978–1002, doi:10.1175/1520-0493(1992)120<0978:RASAPO>2.0.CO;2.

Mueller, B., and S. I. Seneviratne, 2012: Hot days induced by precipitation deficits at the global scale. *Proc. Natl. Acad. Sci. USA,* **109,** 12 398–12 403, doi:10.1073/pnas.1204330109.

Nakamura, H., M. Nakamura, and J. L. Anderson, 1997: The role of high- and low-frequency dynamics and blocking formation. *Mon. Wea. Rev.,* **125,** 2074–2093, doi:10.1175/1520-0493(1997)125<2074:TROHAL>2.0.CO;2.

Nandintsetseg, B., J. S. Greene, and C. E. Goulden, 2007: Trends in extreme daily precipitation and temperature near Lake Hövsgöl, Mongolia. *Int. J. Climatol.,* **27,** 341–347, doi:10.1002/joc.1404.

Nascimento, E. L., and T. Ambrizzi, 2002: The influence of atmospheric blocking on the Rossby wave propagation in Southern Hemisphere winter flows. *J. Meteor. Soc. Japan,* **80,** 139–159, doi:10.2151/jmsj.80.139.

Nesterov, V. G., 1949: *Combustibility of the Forest and Methods for Its Determination* (in Russian). USSR State Industry Press, 76 pp.

Obukhov, A. M., M. V. Kurganskii, and M. S. Tatarskaya, 1984: Dynamical conditions of drought and other large-scale weather anomalies formation (in Russian). *Sov. Meteor. Hydrol.,* **10,** 5–13.

Otto, F. E. L., N. Massey, G. J. van Oldenborgh, R. G. Jones, and M. R. Allen, 2012: Reconciling two approaches to attribution of the 2010 Russian heat wave. *Geophys. Res. Lett.,* **39,** L04702, doi:10.1029/2011GL050422.

Parry, M. L., and Coauthors, Eds., 2007: *Climate Change 2007: Impacts, Adaptation and Vulnerability.* Cambridge University Press, 976 pp.

Pawson, S., R. S. Stolarski, A. R. Douglass, P. A. Newman, J. E. Nielsen, S. M. Frith, and M. L. Gupta, 2008: Goddard Earth Observing System chemistry-climate model simulations of stratospheric ozone-temperature coupling between 1950 and 2005. *J. Geophys. Res.,* **113,** D12103, doi:10.1029/2007JD009511.

Ped, D. A., 1975: On indicators of droughts and wet conditions (in Russsian). *Proc. USSR Hydrometeor. Centre,* **156,** 19–39.

Pines, Y., 2012: *The Everlasting Empire: The Political Culture of Ancient China and Its Imperial Legacy.* Princeton University Press, 248 pp.

Polozova, L. G., and A. A. Grigoryeva, 1984: Role of circulation factor in formation of dry periods, Helio-physical factors of weather and climate. *Proc. A. I. Voeikov Main Geophys. Obs.,* **471,** 50–54.

Potop, V., and M. P. Možný, 2011: Příspěvek ve sborníku (mimo kategorie RIV) [The application of a new drought index—Standardized precipitation evapotranspiration index in the Czech Republic]. *Mikroklima a Mezoklima Krajinných Struktur a Antropogenních Prostředí,* H. Středová, J. Rožnovský, and T. Litschmann, Eds., Český Hydrometeorologický Ústav. [Available online at http://www.cbks.cz/SbornikSMlyn11/Potop1.pdf.]

Protserov, A. V., 1950: Drought in the European territory of the Soviet Union (in Russian). *Agroclimatic Conditions of Steppes of the Ukrainian SSR and Ways to Improve Them* (in Russian), Academy of Sciences of the Ukrainian SSR, 17–22.

Rahmstorf, S., and D. Coumou, 2011: Increase of extreme events in a warming world. *Proc. Natl. Acad. Sci. USA,* **108,** 17 905–17 909, doi:10.1073/pnas.1101766108.

Rayner, N. A., D. E. Parker, E. B. Horton, C. K. Folland, L. V. Alexander, D. P. Rowell, E. C. Kent, and A. Kaplan, 2003: Global analyses of sea surface temperature, sea ice, and night marine air temperature since the late nineteenth century. *J. Geophys. Res.,* **108,** 4407, doi:10.1029/2002JD002670.

Richman, M. B., 1986: Rotation of principal components. *J. Climatol.,* **6,** 293–335, doi:10.1002/joc.3370060305.

Rienecker, M. M., and Coauthors, 2008: The GEOS-5 Data Assimilation System—Documentation of versions 5.0.1, 5.1.0, and 5.2.0. Tech. Rep. Series on Global Modeling and Data Assimilation, Vol. 27, NASA/TM-2008-104606, 95 pp.

——, and Coauthors, 2011: MERRA—NASA's Modern-Era Retrospective Analysis for Research and Applications. *J. Climate,* **24,** 3624–3648, doi:10.1175/JCLI-D-11-00015.1.

Robock, A., K. Y. Vinnikov, G. Srinivasan, J. K. Entin, S. E. Hollinger, N. A. Speranskaya, S. Liu, and A. Namkhai, 2000: The Global Soil Moisture Data Bank. *Bull. Amer. Meteor. Soc.,* **81,** 1281–1299, doi:10.1175/1520-0477(2000)081<1281:TGSMDB>2.3.CO;2.

——, M. Mu, K. Vinnikov, I. V. Trofimova, and T. I. Adamenko, 2005: Forty-five years of observed soil moisture in the Ukraine: No summer desiccation (yet). *Geophys. Res. Lett.,* **32,** L03401, doi:10.1029/2004GL021914.

Rocheva, E. V., 2012: Possible forerunners of droughts in agricultural areas of Russia. *Russ. Meteor. Hydrol.,* **37,** 575–585.

Rudenko, A. I., Ed., 1958: *Droughts in the USSR: Their Origin, Frequency of Occurrence and Impact on Yield* (in Russian). Gidrometeoizdat, 206 pp.

Sato, N., and M. Takahashi, 2006: Dynamical processes related to the appearance of quasi-stationary waves on the subtropical jet in the midsummer Northern Hemisphere. *J. Climate,* **19,** 1531–1544, doi:10.1175/JCLI3697.1.

Scaife, A. A., T. Woollings, J. Knight, G. Martin, and T. Hinton, 2010: Atmospheric blocking and mean biases in climate models. *J. Climate,* **23,** 6143–6152, doi:10.1175/2010JCLI3728.1.

Schneidereit, A., S. Schubert, P. Vargin, F. Lunkeit, X. Zhu, D. H. W. Peters, and K. Fraedrich, 2012: Large-scale flow and the long-lasting blocking high over Russia: Summer 2010. *Mon. Wea. Rev.,* **140,** 2967–2981, doi:10.1175/MWR-D-11-00249.1.

Schubert, S., and Coauthors, 2009: A U.S. CLIVAR project to assess and compare the responses of global climate models to drought-related SST forcing patterns: Overview and results. *J. Climate,* **22,** 5251–5272, doi:10.1175/2009JCLI3060.1.

——, H. Wang, and M. Suarez, 2011: Warm season subseasonal variability and climate extremes in the Northern Hemisphere: The role of stationary Rossby waves. *J. Climate,* **24,** 4773–4792, doi:10.1175/JCLI-D-10-05035.1.

Sedláček, J., O. Martius, and R. Knutti, 2011: Influence of subtropical and polar sea-surface temperature anomalies on temperatures in Eurasia. *Geophys. Res. Lett.,* **38,** L12803, doi:10.1029/2011GL047764.

Selianinov, G. T., 1928: On agricultural climate evaluation (in Russian). *Proc. Agric. Meteor.,* **20,** 165–177.

Seneviratne, S. I., D. Lüthi, M. Litschi, and C. Schär, 2006: Land–atmosphere coupling and climate change in Europe. *Nature,* **443,** 205–209, doi:10.1038/nature05095.

Shver, Ts. A., 1976: *Atmospheric Precipitation over the USSR Territory* (in Russian). Gidrometeoizdat, 302 pp.

Sinor, D., Ed., 1994: *The Cambridge History of Early Inner Asia.* Cambridge University Press, 518 pp.

Smith, T. M., and Coauthors, 2008: Improvements to NOAA's historical merged land–ocean surface temperature analysis (1880–2006). *J. Climate,* **21,** 2283–2293, doi:10.1175/2007JCLI2100.1.

Stankūnavičius, G., D. Basharin, and D. Pupienis, 2012: Relationship between Eurasian large-scale patterns and regional climate variability over the Black and Baltic Seas. *Boreal Environ. Res.,* **17,** 327–346. [Available online at http://www.borenv.net/BER/ber175.htm#327.]

Stefanon, M., F. D'Andrea, and P. Drobinski, 2012: Heatwave classification over Europe and the Mediterranean region. *Environ. Res. Lett.,* **7,** 014023, doi:10.1088/1748-9326/7/1/014023.

Strashnaya, A. I., and N. A. Bogomolova, 2005: On the catalog of severe droughts of soils sown with early spring grain crops in the chernozem zone of Russia (in Russian). *Trans. Russ. Hydrometeor. Res. Center,* **340,** 35–47.

Tang, Q., and G. Leng, 2012: Damped summer warming accompanied with cloud cover increase over Eurasia from 1982 to 2009. *Environ. Res. Lett.,* **7,** 014004, doi:10.1088/1748-9326/7/1/014004.

——, and ——, 2013: Changes in cloud cover, precipitation, and summer temperature in North America from 1982 to 2009. *J. Climate,* **26,** 1733–1744, doi:10.1175/JCLI-D-12-00225.1.

——, ——, and P. Ya. Groisman, 2012: European hot summers associated with a reduction of cloudiness. *J. Climate,* **25,** 3637–3644, doi:10.1175/JCLI-D-12-00040.1.

Thompson, D. W. J., and J. M. Wallace, 2001: Regional climate impacts of the Northern Hemisphere annular mode. *Science,* **293,** 85–89, doi:10.1126/science.1058958.

Ting, M., and L. Yu, 1998: Steady response to tropical heating in wavy linear and nonlinear baroclinic models. *J. Atmos. Sci.,* **55,** 3565–3582, doi:10.1175/1520-0469(1998)055<3565:SRTTHI>2.0.CO;2.

Trenberth, K. E., and J. T. Fasullo, 2012: Climate extremes and climate change: The Russian heat wave and other climate extremes of 2010. *J. Geophys. Res.,* **117,** D17103, doi:10.1029/2012JD018020.

TsUEG, 1933: Opyt predvaritelnogo analiza vosmi katastrophicheskix zasyx za poslednii sorok let (Experience of preliminary analysis of the eight catastrophic droughts for the last forty years), Part 1. Unified Hydrometeorological Sevice of the USSR (TsUEG), 46 pp.

Tyrlis, E., and B. J. Hoskins, 2008: Aspects of a Northern Hemisphere atmospheric blocking climatology. *J. Atmos. Sci.,* **65,** 1638–1652, doi:10.1175/2007JAS2337.1.

Vámbéry, A., 1886: *The Story of the Nations: Hungary.* G. P. Putnam, 453 pp.

van der Schrier, G., K. R. Briffa, P. D. Jones, and T. J. Osborn, 2006: Summer moisture variability across Europe. *J. Climate,* **19,** 2818–2834, doi:10.1175/JCLI3734.1.

Vannari, P. I., 1911: Meteorological networks in Russia and other countries (in Russian). *Meteorological Papers in the Memory of the Chief of the Meteorological Committee of Imperator Russian Geography Society A. I. Voeikov,* Vol. 1, 51–64.

Vautard, R., and Coauthors, 2007: Summertime European heat and drought waves induced by wintertime Mediterranean rainfall deficit. *Geophys. Res. Lett.,* **34,** L07711, doi:10.1029/2006GL028001.

Vazhov, V. I., 1961: Drought frequency over the Russian plain in the historical period (in Russian). Rep. of Crimea Dept. of the Russian Geographical Society of Simpheropol, Vol. 7, 5–17.

Vicente-Serrano, S. M., S. Beguería, and J. I. López-Moreno, 2010: A multi-scalar drought index sensitive to global warming: The standardized precipitation evapotranspiration index. *J. Climate,* **23,** 1696–1718, doi:10.1175/2009JCLI2909.1.

Volodin, E. M., 2011: The nature of some of the strongest summer heat waves (in Russian). *Analysis of Abnormal Weather Conditions in Russia in Summer 2010* (in Russian), N. P. Shakina, Ed., Triada, 48–57.

Wells, N., S. Goddard, and M. J. Hayes, 2004: A self-calibrating Palmer Drought Severity Index. *J. Climate,* **17,** 2335–2351, doi:10.1175/1520-0442(2004)017<2335:ASPDSI>2.0.CO;2.

Woollings, T. J., B. J. Hoskins, M. Blackburn, and P. Berrisford, 2008: A new Rossby wave-breaking interpretation of the North Atlantic Oscillation. *J. Atmos. Sci.,* **65,** 609–626, doi:10.1175/2007JAS2347.1.

Wu, Z., J. Li, Z. Jiang, J. He, and X. Zhu, 2012: Possible effects of the North Atlantic Oscillation on the strengthening relationship between the East Asian summer monsoon and ENSO. *Int. J. Climatol.,* **32,** 794–800, doi:10.1002/joc.2309.

Zampieri, M., F. D'Andrea, R. Vautard, P. Ciais, N. de Noblet-Ducoudré, and P. Yiou, 2009: Hot European summers and the role of soil moisture in the propagation of Mediterranean drought. *J. Climate,* **22,** 4747–4758, doi:10.1175/2009JCLI2568.1.